Copyright Warning & Restrictions

The copyright law of the United States (Title 17, United States Code) governs the making of photocopies or other reproductions of copyrighted material.

Under certain conditions specified in the law, libraries and archives are authorized to furnish a photocopy or other reproduction. One of these specified conditions is that the photocopy or reproduction is not to be "used for any purpose other than private study, scholarship, or research." If a, user makes a request for, or later uses, a photocopy or reproduction for purposes in excess of "fair use" that user may be liable for copyright infringement,

This institution reserves the right to refuse to accept a copying order if, in its judgment, fulfillment of the order would involve violation of copyright law.

Please Note: The author retains the copyright while the New Jersey Institute of Technology reserves the right to distribute this thesis or dissertation

Printing note: If you do not wish to print this page, then select "Pages from: first page # to: last page #" on the print dialog screen

NJIT New Jersey's Science & Technology University

The Van Houten library has removed some of the personal information and all signatures from the approval page and biographical sketches of theses and dissertations in order to protect the identity of NJIT graduates and faculty.

ABSTRACT

GABOR EXPANSION OF AN EQUIVALENT DIPOLE ANTENNA

by
Oksana Manzhura

The Gabor representation in the context of an aperture problem is an expansion of a radiated field in terms of a discrete set of linearly shifted and spatially rotated elementary Gaussian beams. The parameters that can be varied in this summation are the number of beams and corresponding beam widths. As the difficulty associated with the unique determination of the expansion coefficients was alleviated, the method has been successfully applied to one and two dimensional apertures. Although, the asymptotic evaluation of expansion functions has reduced the computational burden drastically, it was at the expense of some loss in accuracy. The numerical experiments have established that the narrow beam algorithm with almost a priori predictability can be used in a variety of problems. Here, the Gabor representation has been applied to a narrow rectangular aperture illuminated with a sinusoidal field. The narrow aperture ($height >> width$) excited by sinusoidal field distribution approximates an equivalent dipole with a similar current distribution with only exception that aperture radiates into a half-space whereas the dipole covers the entire space. Utilizing the narrow beam algorithm, once the expansion coefficients were determined, the radiated electric field potential in near, mid and far zones were evaluated. The criteria in determining the number of expansion coefficients was based on re-generation of the aperture field distribution with sufficient accuracy. It was observed that even though wide beam algorithm was applied, less number of terms resulted in erroneous side

lobes and higher number of terms caused Gibbs phenomena in the region close to the aperture plane. The numerical evaluations are carried out for the half-wavelength high narrow aperture. Far zone numerical results of radiated potential utilizing Gabor expansion are compared to analytical expressions determined via Fourier transform. The unique application developed in this work in expressing the radiated field of an equivalent dipole antenna revealed that Gabor expansion can be a valuable tool in studying practical radiation and propagation problems.

GABOR EXPANSION OF AN EQUIVALENT DIPOLE ANTENNA

by
Oksana Manzhura

A Thesis
Submitted to the Faculty of
New Jersey Institute of Technology
in Partial Fulfillment of the requirements for the Degree of
Master of Science in Electrical Engineering

Department of Electrical and Computer Engineering

January 1996

APPROVAL PAGE

GABOR EXPANSION OF AN EQUIVALENT DIPOLE ANTENNA

Oksana Manzhura

Dr. Edip Niver, Thesis Adviser — Date
Associate Professor of Electrical Engineering, NJIT

Dr. Gerald Whitman, Committee Member — Date
Professor of Electrical Engineering, NJIT

Dr. Ali Akansu, Committee Member — Date
Associate Professor of Electrical Engineering, NJIT

BIOGRAPHICAL SKETCH

Author: Oksana Manzhura

Degree: Master of Science in Electrical Engineering

Date: January 1996

Date of Birth:

Place of Birth:

Undergraduate and Graduate Education:

- Master of Science in Electrical Engineering,
  New Jersey Institute of Technology, Newark, NJ, 1996

- Bachelor of Science in Electrical Engineering,
  New Jersey Institute of Technology, Newark, NJ, 1994

Major: Electrical Engineering

This thesis is dedicated to my parents
Augusta and Yuriy Manzhura
for all their support and guidance
throughout my life .

ACKNOWLEDGMENT

The author wished to express her sincere gratitude to her advisor, Dr. Edip Niver, for his guidance, friendship, and support throughout this research.

Special thanks are extended to Dr. Gerald Whitman and Dr. Ali Akansu for serving as members of the committee.

TABLE OF CONTENTS

Chapter		Page
1	INTRODUCTION	1
2	GABOR REPRESENTATION IN THREE DIMENSIONS	4
	2.1 Formulation	4
	2.2 Evaluation of Gabor Expansion	10
	2.3 Expansion Coefficients $A_{m,n,p,q}$	12
	2.4 Asymptotic Evaluation of Expansion Functions $B_{m,n,p,q}(x,y,z)$	13
3	GABOR REPRESENTATION OF AN APERTURE FOR A TWO DIMENSIONAL SPACE	19
	3.1 Formulation in a Two Dimensional Space	19
	3.2 Gabor Expansion Evaluation	23
	3.3 Numerical Results for One Dimensional Aperture	24
	3.3.1 Uniform Aperture Distribution	25
	3.3.2 Tapered Aperture Distribution	32
4	NUMERICAL RESULTS FOR TWO DIMENSIONAL APERTURES	36
	4.1 Uniform Aperture Field Distribution	36
	4.2 Tapered Aperture Field Distribution	44
5	GABOR REPRESENTATION OF AN EQUIVALENT DIPOLE	50
	5.1 Radiation from a Linear, Center-fed Dipole Antenna	50
	5.2 Radiation from Narrow Apertures	52
6	CONCLUSIONS	63
	REFERENCES	65

LIST OF TABLES

Table		Page
1	Gabor expansion coefficients for a cosine aperture distribution. The parameters chosen are $-9 \leq m \leq 9$, $-6 \leq n \leq 6$ and $L_o/L=9.0$. Only significant coefficients are retained here	35
2	Gabor Expansion Coefficients for a Rectangular Half-Wavelength Aperture Illuminated by Sinusoidal Field Distribution ($L_{ox}/L_x = \lambda/2 = L_{oy}/L_y$) and $n=q=0$, $\|m\|,\|p\| \leq 5$.	61
3	Gabor Expansion Coefficients for a Narrow Half-Wavelength High Aperture Illuminated by Sinusoidal Field Distribution ($L_{ox}/L_x = \lambda/2 = L_{oy}/L_y = \lambda/200$) and $n=q=0$, $\|m\|,\|p\| \leq 5$	62

LIST OF FIGURES

Figure		Page
1	Geometry For a Two Dimensional Rectangular Aperture in a Three Dimensional Space	5
2	An Aperture in Two Dimensional Space.	20
3	Gamma Function $\gamma(x-mL)$ Versus Its Argument	26
4	Pulsed and Tapered (Cosine) Aperture Field Distributions	27
5	Expansion Coefficients $\lvert A_{m,n} \rvert$ for a Pulsed Aperture for Various Values of L_o/L	28
6	A Gabor Representation (— solid line) of a Pulsed Aperture (- - dashed line) with $L_o/L=0.2$ and $-9 \le m \le 9$ and Various Values Versus n	29
7	A Gabor Representation (— solid line) of a Pulsed Aperture (- - dashed line) with $L_o/L=9.0$ and $-9 \le m \le 9$ and Various Values Versus n	30
8	Far Field Distribution of a Pulsed Aperture for Various Values of Observation Point z. (— solid line) Gabor Representation $-9 \le m \le 9$, $-11 \le n \le 11$, in (c) the theoretical far field expression (- - dashed line) was obtained from a Fourier Transform of an Aperture Field	31
9	A Gabor Representation (— solid line) of a Tapered Cosine Aperture Distribution for $L_o/L=9.0$, $-9 \le m \le 9$ and various values versus n	33
10	Far Field Distribution of a Cosine Aperture for Various Values of Observation Point z. (— solid line) Gabor Representation $-9 \le m \le 9$, $-11 \le n \le 11$	34
11	Two Dimensional Gamma Function $\gamma(x-mL_x, y-pL_y)$ Versus its Arguments	37
12	Gabor Coefficients $\lvert A_{m,n,p,q} \rvert$ of the Pulsed Aperture for n=q=0 Versus m and p	40
13	A Gabor Representation of a Pulsed Two Dimensional Aperture Distribution $L_o/L=0.2$ for $\lvert m \rvert, \lvert n \rvert, \lvert p \rvert, \lvert q \rvert \le 9$	41
14	A Gabor Representation of a Pulsed Two Dimensional Aperture Distribution $L_o/L=9.0$ for $\lvert m \rvert, \lvert n \rvert, \lvert p \rvert, \lvert q \rvert \le 9$	42

LIST OF FIGURES
(Continued)

Figure		Page
15	Potential Distribution Due to a Pulsed Aperture in the Near Zone $z=10\lambda$ for $L_{ox}/L_x=L_{oy}/L_y=9.0$ and $\|m\|,\|p\| \leq 9$ $\|n\|,\|q\|=0$	43
16	Potential Distribution of the Pulsed Aperture in the Far Zone $z=100\lambda$ (a) Gabor Summation for $L_{ox}/L_x=L_{oy}/L_y=9.0$ and $\|m\|,\|p\| \leq 9$ (b) Fourier Transform	46
17	Logarithmic Plot of Potential Distribution of the Pulsed Aperture in the Far Zone $z=100\lambda$ (a) Gabor Summation for $L_{ox}/L_x=L_{oy}/L_y=9.0$ and $\|m\|,\|p\| \leq 9$ (b) Fourier Transform	47
18	Gabor Representation of Two Dimensional Cosine Aperture Distribution $L_{ox}/L_x=10.0$ $L_{oy}/L_y=6.0$ for $\|m\|,\|n\|,\|p\|,\|q\| \leq 9$	48
19	Far Field Distribution of a Cosine Aperture for Various Values of Observation Point z on $\varphi=0$ and $\varphi=\pi/2$ Planes. Gabor Representation Parameters are $L_{ox}/L_x=10.0$ and $L_{oy}/L_y=6.0$ $\|m\|,\|p\| \leq 9$ $\|n\|,\|q\|=0$. Solid Lines (—) are Obtained by Gabor Expansion and (- - dashed line) by Fourier Transform (equation (95))	49
20	Geometry of a Linear, Center-Fed Antenna	51
21	Sinusoidal Field Distribution of a Half-Wavelength Rectangular Aperture ($L_{ox}/L_x=\lambda/2=L_{oy}/L_y=\lambda/2$) (a) Plot of the Aperture Field (b) Gabor Representation of the Aperture Field for $n=q=0$, $\|m\|,\|p\| \leq 5$	54
22	Sinusoidal Field Distribution of a Narrow Half-Wavelength Rectangular Aperture ($L_{ox}/L_x=\lambda/2$ $L_{oy}=\lambda/200$ and $L_x=L_y$) (a) Plot of the Aperture Field (b) Gabor Representation of the Aperture Field for $n=q=0$, $\|m\|,\|p\| \leq 5$	55
23	Amplitude of the Electric Potential of a Square Aperture ($L_{ox}/L_x=\lambda/2$, $L_{oy}/L_y=\lambda/2$) Excited by a Sinusoidal Field Illumination. Gabor Parameters are $n=q=0$, $\|m\|,\|p\| \leq 5$ Solid Lines (—) are Obtained by Gabor Expansion and Dashed Lines (- -) Represent Theoretical Results for an Electric Dipole	56

LIST OF FIGURES
(Continued)

Figure — Page

24 Amplitude of the Electric Potential of a Narrow Aperture ($L_{ox}/L_x=\lambda/2=L_{oy}/L_y=\lambda/200$) Excited by a Sinusoidal Field Illumination. Gabor Parameters are n=q=0, |m|,|p| ≤5. Solid Lines (—) are Obtained by Gabor Expansion and Dashed Lines (- -) Represent Theoretical Results for an Electric Dipole 57

25 Amplitude of the Electric Potential of an Equivalent Dipole. A Narrow Aperture of a Sinusoidal Field Distribution ($L_{ox}/L_x=\lambda/2$ $L_{oy}=\lambda/200$) Gabor Parameters are n=q=0, |m|,|p| ≤ 5 $L_y=L_x=0.1$ Solid Lines (—) are Obtained by Gabor Expansion and Dashed Lines (- -) Represent Theoretical Results for an Electric Dipole 58

26 Amplitude of the Electric Potential of an Equivalent Dipole. A Narrow Aperture of a Sinusoidal Field Distribution ($L_{ox}/L_x=\lambda/2$ $L_{oy}=\lambda/200$) Gabor Parameters are n=q=0, |m|,|p| ≤ 5 $L_y=L_x=0.2$ Solid Lines (—) are Obtained by Gabor Expansion and Dashed Lines (- -) Represent Theoretical Results for an Electric Dipole 59

27 Amplitudes of the Electric Field Potential for the Far Zone ($z=100\lambda$) of an Equivalent Half-Wavelength Dipole at $\varphi=0$ plane. Gabor Parameters are $L_y=L_x=0.1$ p=q=0 60

CHAPTER 1

INTRODUCTION

The Gabor representation consists of an expansion of a signal into a discrete set functions which are finite duration both in time and frequency [1]. The method was proposed by Gabor in 1946, however, applications were very limited because of difficulties associated with evaluations of the expansion coefficients. Major contributions in early 1980's by Bastiaans [2]-[3] and Janssen [4] helped to alleviate this difficulty and led to a methodical approach in determination of the expansion coefficients. The Gabor representation in the context of an aperture problem [5] is an expansion of a radiated field in terms of a discrete set of linearly shifted and spatially rotated elementary Gaussian beams. The parameters that can be varied in this summation are the number of beams and corresponding beam widths. As the difficulty associated with the unique determination of the expansion coefficients was alleviated, the method has been successfully applied to one and two dimensional apertures. Though the initial formulation for two dimensional apertures was developed by Einziger, et.al. [5], detailed analysis and extensive numerical evaluations were carried out by Maciel [6]. He further extended Gaussian beam method for propagation of high frequency fields from distributed apertures through complicated environments such as radomes. Although, utilizing the complex source point method, the asymptotic evaluation of expansion functions has reduced the computational burden drastically, it was at the expense of some loss in accuracy. The numerical experiments have established that

the narrow beam algorithm with almost a priori predictability can be used in a variety of problems.

Here, the Gabor representation has been applied to a narrow rectangular aperture illuminated with a sinusoidal field. The narrow aperture ($height >> width$) excited by sinusoidal field distribution approximates an equivalent dipole with a similar current distribution with only exception that aperture radiates into a half-space whereas the dipole covers the entire space. In the past, this approach had been successfully applied using spherical wave functions by Niver and Birand [7]. One advantage of representing the radiated field in terms of an expansion is that once the expansion coefficients are determined, field can be evaluated using summation of the finite number of terms without further need of repeated evaluation of the spectral integral for every observation point. In the case of spherical wave expansions, the multipole coefficients of a linear dipole were already determined analytically by Jackson [8]. The validity of the spherical expansion method was double checked, initially the known coefficients of a dipole were compared to those of the narrow aperture, then the radiated fields were compared for both antennas.

In the current approach, the expansion coefficient of the Gabor representation can not be validated independently, since there is no known benchmark solution. However, radiated field from the narrow rectangular aperture has been determined utilizing the narrow beam algorithm, once the expansion coefficients are determined, the radiated electric field potential in near, mid and far zones is evaluated. The criteria in determining the number of expansion coefficients is based on re-generation of the aperture field distribution with sufficient accuracy. It was observed that even though

narrow beam algorithm was applied, less number of terms resulted in erroneous side lobes and higher number of terms caused Gibbs phenomena in the region close to the aperture plane. The numerical evaluations are carried out for the half-wavelength high narrow aperture. Far zone numerical results of radiated potential utilizing Gabor expansion are compared to analytical expressions determined via Fourier transform. The unique application developed in this work in expressing the radiated field of an equivalent dipole antenna revealed that Gabor expansion can be a valuable tool in studying practical radiation and propagation problems.

In Chapter II the three dimensional Gabor representation has been presented, techniques on evaluation of expansion coefficients and asymptotically treated beam functions have been outlined. Chapter III summarizes the two dimensional formulation and numerical examples confirming of the validity of the narrow beam algorithm are presented. The equivalent dipole antenna concept based on narrow aperture is developed and its validity in the context of Gabor representation is illustrated with various numerical results in Chapter IV. The conclusions and suggestions for future work are presented in Chapter V.

CHAPTER 2

GABOR REPRESENTATION IN THREE DIMENSIONS

The Gabor representation consists of an expansion of a signal into a discrete set of Gaussian expansion functions [1]. However, applications of Gabor representation was limited because of difficulties associated with computing the expansion coefficients. Contributions by Bastiaans [2],[3] and Janssen[4] helped to remove these difficulties and led to concrete approach to determine these expansion coefficients. Then, the Gabor expansion was successfully applied to an aperture problem [5], though formulation in three dimensions was formulated, extensive numerical results were presented only in two dimensions. The Gabor expansion in three dimensions was studied in detail by Maciel [6], where Gaussian beam summations in two and three dimensions were applied in complicated environments. In this chapter, the three dimensional Gabor expansion will be reviewed within the context of an aperture problem.

2.1 Formulation

In the three dimensional space, it is assumed that an arbitrary polarized aperture field distribution with suppressed $e^{-i\omega t}$ variation exists on the $z = 0$ plane as shown in Figure 1. The transverse aperture field distribution can be described as

$$\mathbf{E}(x, y, 0) = \mathbf{E}(x, y, z) \mid_{z=0} = \mathbf{f}_t(x, y) \tag{1}$$

where $\mathbf{f}_t(x, y)$ is a vector function of spacial variables x and y as shown in formula (2)

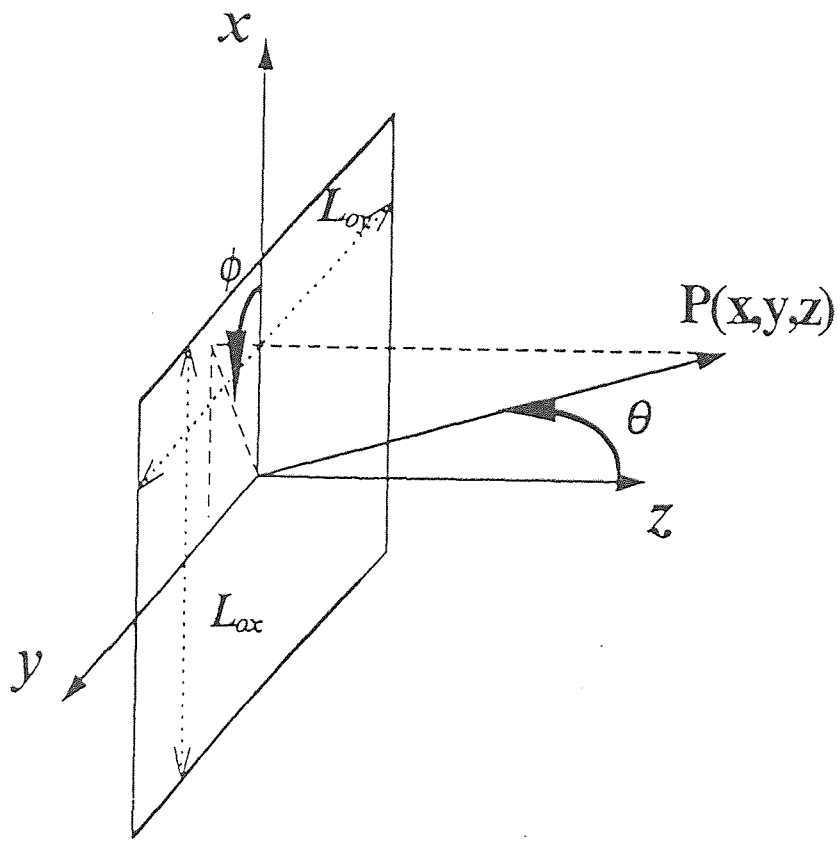

Figure 1. Geometry for a two dimensional rectangular aperture in a three dimensional space.

$$\mathbf{f}_t(x,y) = \hat{x} f_{t_x}(x,y) + \hat{y} f_{t_y}(x,y) \tag{2}$$

Two dimensional Fourier transform (plane wave spectrum representation) of the functional dependence of the aperture field is

$$\mathbf{F}_t(\eta,\xi) = \iint_{-\infty}^{\infty} \mathbf{f}_t(x,y) e^{-i(\eta x + \xi y)} dx dy \tag{3}$$

The field distribution at any point $P(x,y,z)$, $z > 0$ can be represented as a superposition of plane waves (plane wave spectrum)

$$\mathbf{E}(\mathbf{r}) = \mathbf{E}(x,y,z) = \frac{1}{(2\pi)^2} \iint_{-\infty}^{\infty} \mathbf{F}(\eta,\xi) e^{i\mathbf{k}\cdot\mathbf{r}} d\eta d\xi \tag{4}$$

where

$$\mathbf{F}(\eta,\xi) = \mathbf{F}_t(\eta,\xi) - \hat{z} \frac{\mathbf{k}\cdot\mathbf{F}_t}{\kappa} \tag{5}$$

with wave number vector $\mathbf{k}$

$$\mathbf{k} = \hat{x}\eta + \hat{y}\xi + \hat{z}\kappa \tag{6}$$

and position vector $\mathbf{r}$

$$\mathbf{r} = \hat{x}x + \hat{y}y + \hat{z}z \tag{7}$$

and $\kappa = \sqrt{k^2 + \eta^2 + \xi^2}$, $Re\{\kappa\} \geq 0$ and $Im\{\kappa\} \geq 0$. The vector potential expression for electric field at point $P(x,y,z)$ is

$$\mathbf{E}(\mathbf{r}) = \nabla \times \bar{\psi}(\mathbf{r}) \tag{8}$$

Substituting (4) into (3), it is possible to express this potential as

$$\bar{\psi}(\mathbf{r}) = \frac{i}{(2\pi)^2} \iint_{-\infty}^{\infty} \hat{z} \times \mathbf{F}_t(\eta, \xi) \frac{e^{i\mathbf{k}\cdot\mathbf{r}}}{\kappa} d\eta d\xi \tag{9}$$

or in terms of $\mathbf{f}_t(x, y)$

$$\bar{\psi}(\mathbf{r}) = \frac{1}{2\pi} \iint_{-\infty}^{\infty} \hat{z} \times \mathbf{f}_t(x, y) \frac{e^{ikR}}{R} dx' dy' \tag{10}$$

where the distance parameter R is

$$R = \sqrt{(x - x')^2 + (y - y')^2 + z^2} \tag{11}$$

The aperture field may be represented by a fourfold Gabor spectral expansion as

$$\mathbf{f}_t(x, y) = \sum_{m,n,p,q} \mathbf{A}_{m,n,p,q} w(x - mL_x, y - pL_y) e^{i(n\Omega_x x + q\Omega_y y)} \tag{12}$$

where

$$\Omega_x = \frac{2\pi}{L_x} \qquad \Omega_y = \frac{2\pi}{L_y} \tag{13}$$

and index m is related to spatial shift in $\hat{x}$ direction, p is related to spatial shift in $\hat{y}$ direction, n and q denote spectral tilts. The Fourier transform of the aperture distribution (substituting (8) into (2) and changing the order of integration and summation) leads to

$$\mathbf{F}_t(\eta,\xi) = \sum_{m,n,p,q} \mathbf{A}_{m,n,p,q} W(\eta - n\Omega_x, \xi - q\Omega_y) e^{-i(mL_x\eta + pL_y\xi)} \tag{14}$$

where $W(\eta,\xi)$ is a two dimensional Fourier transform of Gaussian finite-energy window function

$$w(x,y) = \sqrt{\frac{2}{L_x L_y}} e^{-\pi(\frac{x^2}{L_x^2} + \frac{y^2}{L_y^2})} \tag{15}$$

and its transform is

$$W(\eta,\xi) = \iint_{-\infty}^{\infty} w(x,y) e^{-i(\eta x + \xi y)} dx dy \tag{16}$$

Substituting (15) in (16) yields

$$W(\eta,\xi) = 2\pi \sqrt{\frac{2}{\Omega_x \Omega_y}} e^{-\pi(\frac{\eta^2}{\Omega_x^2} + \frac{\xi^2}{\Omega_y^2})} \tag{17}$$

The elementary beam representation in general form can be expressed as

$$\bar{\psi}(\mathbf{r}) = \sum_{m,n,p,q} \hat{z} \times \mathbf{A}_{m,n,p,q} B_{m,n,p,q} \tag{18}$$

where

$$B_{m,n,p,q} = \frac{i}{(2\pi)^2} \iint_{-\infty}^{\infty} W(\eta - n\Omega_x, \xi - q\Omega_y) \frac{e^{i[(x-mL_x)\eta + (y-pL_y)\xi]}}{\kappa} d\eta d\xi \tag{19}$$

or

$$B_{m,n,p,q} = \frac{1}{2\pi} \iint_{-\infty}^{\infty} w(x' - mL_x, y' - pL_y) e^{i(n\Omega_x x' + q\Omega_y y')} \frac{e^{ikR}}{R} dx' dy' \tag{20}$$

The Gabor coefficients $\mathbf{A}_{m,n,p,q}$ can be determined by means of the function $\gamma(x,y)$

obeying biorthogonality conditions

$$\iint_{-\infty}^{\infty} w(x,y)\gamma^*(x-mL_x, y-pL_y)e^{-i(n\Omega_x x+q\Omega_y y)}dxdy = \delta_m\delta_n\delta_p\delta_q \tag{21}$$

or

$$\frac{1}{2\pi}\iint_{-\infty}^{\infty} W(\eta,\xi)\Gamma^*(\eta-n\Omega_x, \xi-q\Omega_y)e^{i(mL_x\eta+pL_y\xi)}d\eta d\xi = \delta_m\delta_n\delta_p\delta_q \tag{21.b}$$

and the completeness relation

$$\sum_{m,n,p,q} w(x-mL_x, y-mL_y)\gamma^*(x'-mL_x, y'-pL_y)e^{i[n\Omega_x(x-x')+q\Omega_y(y-y')]} = \delta(x-x')\delta(y-y') \tag{22}$$

If $\gamma(x,y)$ is known, which is the case for the chosen window function (15) leads to (Appendix A)

$$\gamma(x,y) = \frac{\pi^3}{K_0^3\sqrt{2L_xL_y}}e^{\pi(\frac{x^2}{L_x^2}+\frac{y^2}{L_y^2})}\sum_{i_1\geq\frac{x}{L_x}-\frac{1}{2}}^{\infty}(-1)^{i_1}e^{-\pi(i_1+\frac{1}{2})^2} \tag{23}$$

$$\times\sum_{i_2\geq\frac{y}{L_y}-\frac{1}{2}}^{\infty}(-1)^{i_2}e^{-\pi(i_2+\frac{1}{2})^2}$$

where $K_0 = 1.85407468$ represents the complete elliptic integral of the first kind of argument $1/2$.

The Gabor coefficients can then be determined from

$$\mathrm{A}_{m,n,p,q} = \iint_{-\infty}^{\infty}\mathrm{f}_t(x,y)\gamma^*(x-mL_x, y-pL_y)e^{-i(n\Omega_x x+q\Omega_y y)}dxdy \tag{24}$$

or alternatively

$$\mathbf{A}_{m,n,p,q} = \frac{1}{(2\pi)^2} \iint_{-\infty}^{\infty} \mathbf{F}_t(\eta,\xi)\Gamma^*(\eta - n\Omega_x, \xi - q\Omega_y) e^{-i(mL_x\eta + pL_y\xi)} d\eta d\xi \qquad (25)$$

2.2 Evaluation of Gabor Expansion

Gabor expansion coefficients $\mathbf{A}_{m,n,p,q}$ in the expansion (18) are vector quantities in the transverse plane

$$\mathbf{A}_{m,n,p,q} = \hat{x} A^x_{m,n,p,q} + \hat{y} A^y_{m,n,p,q} \qquad (26)$$

as defined in (24) and (25). The expansion functions $B_{m,n,p,q}$ of the expansion (18) are the elementary beam functions defined in (19) and (20). Substituting Gabor coefficients(26) into the vector potential $\bar{\psi}(\mathbf{r})$ via Gabor representation (18) leads to

$$\bar{\psi}(\mathbf{r}) = \sum_{m,n,p,q} (-\hat{x} A^y_{m,n,p,q} + \hat{y} A^x_{m,n,p,q}) B_{m,n,p,q} \qquad (27)$$

Then the electric field $\mathbf{E}(\mathbf{r})$ can be determined from (18) as

$$\mathbf{E}(\mathbf{r}) = \sum_{m,n,p,q} (-\hat{x} A^x_{m,n,p,q} \frac{\partial B_{m,n,p,q}}{\partial z} - \hat{y} A^y_{m,n,p,q} \frac{\partial B_{m,n,p,q}}{\partial z} + \qquad (28)$$

$$+ \hat{z}(A^x_{m,n,p,q} \frac{\partial B_{m,n,p,q}}{\partial x} + A^y_{m,n,p,q} \frac{\partial B_{m,n,p,q}}{\partial y}))$$

The explicit form of derivatives of elementary beam functions for spectral representation are

$$\frac{\partial B_{m,n,p,q}}{\partial x} = \frac{-1}{(2\pi)^2}\iint_{-\infty}^{\infty} \frac{\eta}{\kappa} W(\eta - n\Omega_x\xi - q\Omega_y) e^{i((x-mL_x)\eta+(y-pL_y)\xi+\kappa z)} d\eta d\xi \tag{29}$$

$$\frac{\partial B_{m,n,p,q}}{\partial y} = \frac{-1}{(2\pi)^2}\iint_{-\infty}^{\infty} \frac{\xi}{\kappa} W(\eta - n\Omega_x\xi - q\Omega_y) e^{i((x-mL_x)\eta+(y-pL_y)\xi+\kappa z)} d\eta d\xi \tag{30}$$

$$\frac{\partial B_{m,n,p,q}}{\partial z} = \frac{-1}{(2\pi)^2}\iint_{-\infty}^{\infty} W(\eta - n\Omega_x\xi - q\Omega_y) e^{i((x-mL_x)\eta+(y-pL_y)\xi+\kappa z)} d\eta d\xi \tag{31}$$

and their spatial representations are

$$\frac{\partial B_{m,n,p,q}}{\partial x} = \frac{1}{2\pi}\iint_{-\infty}^{\infty} \frac{(x-x')(ikR-1)}{R^2} w(x' - mL_x, y' - pL_y)$$

$$\times e^{i(n\Omega_x x' + q\Omega_y y')} \frac{e^{ikR}}{R} dx' dy' \tag{32}$$

$$\frac{\partial B_{m,n,p,q}}{\partial y} = \frac{1}{2\pi}\iint_{-\infty}^{\infty} \frac{(y-y')(ikR-1)}{R^2} w(x' - mL_x, y - pL_y)$$

$$\times e^{i(n\Omega_x x' + q\Omega_y y')} \frac{e^{ikR}}{R} dx' dy' \tag{33}$$

$$\frac{\partial B_{m,n,p,q}}{\partial\ z} = \frac{1}{2\pi}\iint_{-\infty}^{\infty} \frac{z(ikR-1)}{R^2} w(x' - mL_x, y' - pL_y)$$

$$\times e^{i(n\Omega_x x' + q\Omega_y y')} \frac{e^{ikR}}{R} dx' dy' \tag{34}$$

The orientation of the vector of the three dimensional transverse aperture field of equation (1) can be chosen along the $\hat{x}$ direction as a special case

$$\mathbf{f}_t(x,y) = \hat{x} f(x,y) \tag{35}$$

Such a choice leads to a simplified solution for the vector potential and expansion coefficients

$$\mathbf{A}_{m,n,p,q} = \hat{x} A^x_{m,n,p,q} \tag{36}$$

the vector potential

$$\bar{\psi}(\mathbf{r}) = \sum_{m,n,p,q} \hat{y} A^x_{m,n,p,q} B_{m,n,p,q} \tag{37}$$

and the magnitude of the $\bar{\psi}(\mathbf{r})$ is

$$\psi(r) = \left| \sum_{m,n,p,q} A_{m,n,p,q} B_{m,n,p,q} \right| \tag{38}$$

The reduced electric field expression becomes

$$\mathbf{E}(\mathbf{r}) = \sum_{m,n,p,q} -\hat{x} A^x_{m,n,p,q} \frac{\partial B_{m,n,p,q}}{\partial z} + \hat{z} A^x_{m,n,p,q} \frac{\partial B_{m,n,p,q}}{\partial x} \tag{39}$$

2.3 Expansion Coefficients $A_{m,n,p,q}$

The Gabor expansion coefficients $\mathbf{A}_{m,n,p,q}$ are defined in (24) and (25) in terms of space and wave number variables, respectively. The choice of Gaussian finite energy function $w(x, y)$ in (15) leads to a biorthogonal function $\gamma(x, y)$ in (23). Hence, this choice of the Gaussian window function yields a real gamma function $\gamma(x, y)$, which implies that the conjugate operation in (24) and (25) does not alter the solution.

It is possible to recognize that formulas (24) and (25) are Fourier transforms of $\mathbf{f}_t(x, y)\gamma^*(x - mL_x, y - pL_y)$ and of $\mathbf{F}_t(\eta, \xi)\Gamma^*(\eta - n\Omega_x, \xi - q\Omega_y)$ with the conjugate variables $n\Omega_x, q\Omega_y$ and mL_x, pL_y, respectively.

Any two dimensional aperture function distribution would have form of

$$f(x,y) = \begin{cases} f(x,y), & |x| \le \frac{L_{ox}}{2} \quad and \quad |y| \le \frac{L_{oy}}{2} \\ 0, & |x| > \frac{L_{ox}}{2} \quad or \quad |y| > \frac{L_{oy}}{2} \end{cases} \tag{40}$$

Thus the numerical evaluation of Gabor coefficients results in a limited integration over the non-zero aperture distribution

$$\mathbf{A}_{m,n,p,q} = \int_{-L_{0x}/2}^{L_{0x}/2} \int_{-L_{0y}/2}^{L_{0y}/2} \mathbf{f}_t(x,y)\gamma^*(x - mL_x, y - pL_y)e^{-i(n\Omega_x x + q\Omega_y y)}dxdy \tag{41}$$

with biorthogonal Gamma function γ defined as in (23). These coefficients were evaluated by numerical integration in this work.

Once the expansion coefficients are determined, their optimal number for the chosen set of parameters can be estimated by evaluating the aperture distribution using (12). The number of coefficients can be increased until satisfactory agreement of aperture field distribution is achieved.

2.4 Asymptotic Evaluation of Expansion Functions $B_{m,n,p,q}(x,y,z)$

The expansion functions $B_{m,n,p,q}$ in Gabor's representation are defined in (19) and (20) in terms of integral representations. Rather than the extensive numerical evaluation of spectral integrals in (12) and (20), it is worthwhile to evaluate them asymptotically [6]. The asymptotic evaluation of these functions dictates that the observation point should satisfy the far field conditions.

In a double integral, once the saddle point is determined, the integration contour

can be confined to the steepest descent path (SDP)

$$I = \iint_{SDP} g(\zeta_1, \zeta_2) e^{i\Omega f(\zeta_1, \zeta_2)} d\zeta_1 d\zeta_2 \tag{42}$$

where Ω is the large parameter. Integral in (42) can be asymptotically evaluated in the first order as

$$I \sim \frac{2\pi}{i\Omega} g(\zeta_1, \zeta_2) J e^{i\Omega f(\zeta_1, \zeta_2)} \tag{43}$$

The Jacobian J is defined as

$$J = \frac{1}{\sqrt{\frac{\partial^2 f}{\partial \zeta_1^2}\frac{\partial^2 f}{\partial \zeta_2^2} - (\frac{\partial^2 f}{\partial \zeta_1 \partial \zeta_2})^2}} \Big|_{\substack{\zeta_1=\zeta_{1_s} \\ \zeta_2=\zeta_{2_s}}} \tag{44}$$

and the saddle point $(\zeta_{1_s}, \zeta_{2_s})$ satisfies the following equation

$$\frac{\partial f}{\partial \zeta_1} \Big|_{\zeta_1=\zeta_{1_s}} = \frac{\partial f}{\partial \zeta_2} \Big|_{\zeta_2=\zeta_{2_s}} = 0 \tag{45}$$

Applying the following change of variables to equation (19) using the following transformation

$$x - mL_x = \rho \sin\Theta \cos\Phi \tag{46.a}$$

$$y - pL_y = \rho \sin\Theta \sin\Phi \tag{46.b}$$

$$z = \cos\Theta \tag{46.c}$$

$$\rho = \hat{x}(x - mL_x) + \hat{y}(y - pL_y) + \hat{z}z \tag{46.d}$$

and substituting the definition of Fourier transform of the Gaussian window function (17), yields

$$B_{m,n,p,q} = i\frac{\sqrt{2L_xL_y}}{(2\pi)^2}\iint_{-\infty}^{\infty}(k^2 - \eta^2 - \xi^2)^{-1/2}e^{i\rho f(\eta,\xi)}d\eta d\xi \tag{47}$$

Asymptotic approximation of the form (43) will yield

$$B_{m,n,p,q} \sim \frac{\sqrt{2L_xL_y}}{2\pi\rho\sqrt{k^2 - \eta_s^2 - \xi_s^2}}Je^{i\rho f(\eta_s,\xi_s)} \tag{48}$$

where the phase function

$$f(\eta,\xi) = \eta\sin\Theta\cos\Phi + \xi\sin\Theta\cos\Phi + \sqrt{k^2 - \eta^2 - \xi^2}\cos\Theta + \tag{49}$$

$$+\frac{i\pi}{\rho}\left[\frac{(\eta - n\Omega_x)^2}{\Omega_x^2} + \frac{(\xi - q\Omega_y)^2}{\Omega_y^2}\right]$$

The saddle point (η_s, ξ_s) should satisfy the following system of equations

$$\frac{\partial f}{\partial \eta}\,|_{\eta=\eta_s} = \sin\Theta\cos\Phi - \frac{\eta_s\cos\Theta}{\sqrt{k^2 - \eta^2 - \xi^2}} + i\pi\frac{2\eta_s - 2n\Omega_x}{\rho\Omega_x^2} = 0 \tag{50.a}$$

$$\frac{\partial f}{\partial \xi}\,|_{\xi=\xi_s} = \sin\Theta\sin\Phi - \frac{\xi_s\cos\Theta}{\sqrt{k^2 - \eta^2 - \xi^2}} + i\pi\frac{2\xi_s - 2n\Omega_y}{\rho\Omega_y^2} = 0 \tag{50.b}$$

Transforming (50) into original variables leads to

$$\eta_s\frac{(z - i\frac{L_x^2\kappa}{2\pi})}{z - ib} - \epsilon_x\kappa + \frac{i\frac{L_x^2n\Omega_x\kappa}{2\pi}}{z - ib} = 0 \tag{51.a}$$

$$\xi_s \frac{(z - i\frac{L_y^2\kappa}{2\pi})}{z - ib} - \epsilon_y\kappa + \frac{i\frac{L_y^2 q\Omega_y\kappa}{2\pi}}{z - ib} = 0 \tag{51.b}$$

where b is an unknown beam waist parameter and the following variables are defined as $\kappa = \sqrt{k^2 - \eta^2 - \xi^2}$, $\epsilon_x = \frac{x - mL_x}{z - ib}$, and $\epsilon_y = \frac{y - pL_y}{z - ib}$. As can be seen, the asymptotic evaluation of expansion function $B_{m,n,p,q}$ requires a solution of a system of coupled complex equations (51), but it is possible to simplify this task by introducing a complex source point technique. Considering the far field and paraxial approximations, apply a perturbation expansion of a saddle point coordinates up to quadratic terms

$$\eta_s = \eta_0 + \epsilon_x\eta_1 + \epsilon_x^2\eta_2 + O(\epsilon_x^3) \tag{52.a}$$

$$\xi_s = \xi_0 + \epsilon_y\xi_1 + \epsilon_y^2\xi_2 + O(\epsilon_y^3) \tag{52.b}$$

This leads to an approximate solution for the saddle point for the symmetrical $L_x = L_y = L$, non-tilted beams represented by $n = 0$ and $q = 0$

$$\eta_s = \frac{k(x - mL)}{z - \frac{L^2}{\lambda}} \tag{53.a}$$

$$\xi_s = \frac{k(y - pL)}{z - \frac{L^2}{\lambda}} \tag{53.b}$$

and

$$b = \frac{L^2}{\lambda} \tag{54}$$

Non-tilted, propagating beams carry the most of the contribution into the field, this

is why limitation of the solution only to these beams is justified. After substituting solutions (53) into (48)-(49) approximate expansion of the function results in a paraxial approximation

$$B_{m,n,p,q} \sim \frac{\sqrt{2}L}{2\pi(z-i\frac{L^2}{\lambda})} e^{ik(z+\frac{(x-mL)^2+(y-pL)^2}{z-i\frac{L^2}{\lambda}})} \tag{55}$$

A similar complex source point approximation can be extended to the derivatives of expansion functions $B_{m,n,p,q}$. Applying the transformation in (46) to (29-31) yields

$$\frac{\partial B_{m,n,p,q}}{\partial x} = -\frac{\sqrt{2L_xL_y}}{(2\pi)^2} \iint_{-\infty}^{\infty} \eta(k^2-\eta^2-\xi^2)^{-1/2} e^{i\rho f(\eta,\xi)} d\eta d\xi \tag{56}$$

$$\frac{\partial B_{m,n,p,q}}{\partial y} = -\frac{\sqrt{2L_xL_y}}{(2\pi)^2} \iint_{-\infty}^{\infty} \xi(k^2-\eta^2-\xi^2)^{-1/2} e^{i\rho f(\eta,\xi)} d\eta d\xi \tag{57}$$

$$\frac{\partial B_{m,n,p,q}}{\partial z} = -\frac{\sqrt{2L_xL_y}}{(2\pi)^2} \iint_{-\infty}^{\infty} e^{i\rho f(\eta,\xi)} d\eta d\xi \tag{58}$$

which can be approximated utilizing (43) into above relations

$$\frac{\partial B_{m,n,p,q}}{\partial x} \sim -\frac{i\eta\sqrt{2L_xL_y}}{2\pi\rho\sqrt{k^2-\eta_s^2-\xi_s^2}} J e^{i\rho f(\eta_s,\xi_s)} \tag{59}$$

$$\frac{\partial B_{m,n,p,q}}{\partial y} \sim -\frac{i\xi\sqrt{2L_xL_y}}{2\pi\rho\sqrt{k^2-\eta_s^2-\xi_s^2}} J e^{i\rho f(\eta_s,\xi_s)} \tag{60}$$

$$\frac{\partial B_{m,n,p,q}}{\partial z} \sim -\frac{i\sqrt{2L_xL_y}}{2\pi\rho} J e^{i\rho f(\eta_s,\xi_s)} \tag{61}$$

where the Jacobian and the phase function evaluated at the saddle point $f(\eta_s,\xi_s)$ are

identical to (44) and (49), respectively. Hence, derivatives obtained in (29-31) are subject to approximations in symmetry $L_x = L_y = L$ and non-tilted ($n = 0$ and $q = 0$) beams simplify into

$$\frac{\partial B_{m,n,p,q}}{\partial x} \sim -\frac{ik(x-mL)\sqrt{2}L}{2\pi(z-i\frac{L^2}{\lambda})^2} e^{ik(z+\frac{(x-mL)^2+(y-pL)^2}{z-i\frac{L^2}{\lambda}})} \tag{62}$$

$$\frac{\partial B_{m,n,p,q}}{\partial y} \sim -\frac{ik(y-pL)\sqrt{2}L}{2\pi(z-i\frac{L^2}{\lambda})^2} e^{ik(z+\frac{(x-mL)^2+(y-pL)^2}{z-i\frac{L^2}{\lambda}})} \tag{63}$$

$$\frac{\partial B_{m,n,p,q}}{\partial z} \sim -\frac{ik\sqrt{(z-i\frac{L^2}{\lambda})^2-(x-mL)^2-(y-pL)^2}\sqrt{2}L}{2\pi(z-i\frac{L^2}{\lambda})^2} \times e^{ik(z+\frac{(x-mL)^2+(y-pL)^2}{z-i\frac{L^2}{\lambda}})} \tag{64}$$

Hence, an approximate solution for the far-field electric field in (28) can be evaluated using expansion coefficients in (41) and expansion function derivatives in (62)-(64). For the specific choice of an aperture distribution in (35) the far field electric field in (39) can be determined via (36) and (62)-(64).

CHAPTER 3

GABOR REPRESENTATION OF AN APERTURE IN A TWO DIMENSIONAL SPACE

It is possible to reduce the three dimensional theoretical formulation presented in Chapter 2 to an aperture in a two dimensional space. Theoretical analysis and numerical evaluation for this case are very similar to a three dimensional problem [5]. However, physical interpretation is simpler for a two dimensional case without additional complexity of a third dimension.

A very detailed study of analysis and synthesis of aperture, near field and far zone fields by Gabor representation has been carried by Maciel [6]. The behavior of wide, narrow and "matched" beam superposition was investigated, the contribution of each individual beam and certain group of beams to the total field was identified. Here, only a brief overview will be presented.

3.1 Formulation in a Two Dimensional Space

A one dimensional aperture located in a two dimensional space is shown in Figure 2. The aperture field distribution (the transverse electric field) can be chosen without loss of generality to be along the $\hat{y}$ direction as

$$\mathbf{E}(x,z)\mid_{z=0}= \mathbf{E}(x,0) = \mathbf{f}(x) = \hat{y}f(x) \tag{65}$$

It is possible to describe the field in the half space $z \geq 0$ at an observation point

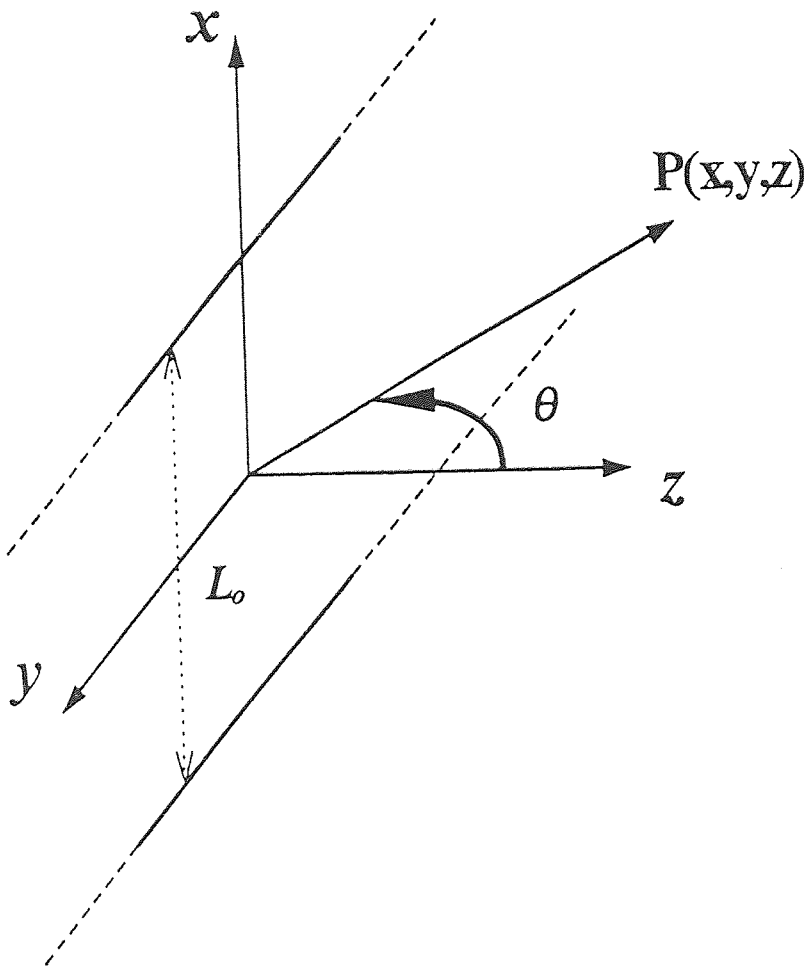

Figure 2. An aperture in two dimensional space.

$P(x,z)$ using plane-wave spectral representation as

$$\mathbb{E}(x,z) = \frac{1}{2\pi}\int_{-\infty}^{\infty} \mathbb{F}(\eta)e^{i(\eta x+\kappa z)}dx \tag{66}$$

where $\mathbb{F}(\eta)$ is the Fourier transform of the functional dependence of the aperture field $\mathbf{f}(x)$

$$\mathbb{F}(\eta) = \int_{-\infty}^{\infty} \mathbf{f}(x)e^{-i\eta x}dx \tag{67}$$

Or it is possible to describe the same field by the point-source response superposition

$$\mathbb{E}(x,z) = \frac{ikz}{2}\int_{-\infty}^{\infty} \mathbf{f}(x')\frac{H_1^{(1)}(kR)}{R}dx' \tag{68}$$

where distance R in (11) is now reduced to

$$R = \sqrt{(x'-x)^2+z^2} \tag{69}$$

and $H_1^{(1)}(kR)$ is a Hankel function of the first kind of order 1.

It is possible to express a Gabor representation of the scalar aperture field function as

$$f(x) = \sum_{m,n} A_{m,n}w(x-mL)e^{in\Omega x} \tag{70}$$

where index m indicates spatial shift and index n a spectral tilt with spatial displacement parameter L, which is a Gaussian beam with waist width and a spectral displacement parameter $\Omega = \frac{2\pi}{L}$.

Finite-energy window function $w(x)$ will be chosen as a normalized Gaussian

$$w(x) = \sqrt{\frac{\sqrt{2}}{L}} e^{-\pi(\frac{x}{L})^2} \tag{71}$$

Using equation (71) in a Fourier transform of an aperture function(67) results in

$$F(\eta) = \sum_{m,n} A_{m,n} W(\eta - n\Omega) e^{-imL\eta} \tag{72}$$

where $W(\eta)$ is a Fourier transform of the window function in (71)

$$W(\eta) = \int_{-\infty}^{\infty} w(x) e^{-i\eta x} dx = \sqrt{\frac{\sqrt{2}2\pi}{\Omega}} e^{\pi(\frac{\eta}{\Omega})^2} \tag{73}$$

Substituting equations (70) and (72) in equations (66) and (68) and changing the order of integration and summation results in an expansion

$$\mathbf{E}(x,z) = \sum_{m,n} \mathbf{A}_{m,n} B_{m,n}(x,z) \tag{74}$$

where elementary beam functions $B_{m,n}(x,z)$ can either be represented spectrally as

$$B_{m,n}(x,z) = \frac{1}{2\pi} \int_{-\infty}^{\infty} W(\eta - n\Omega) e^{i(\eta(x-mL)+\kappa z)} d\eta \tag{75}$$

or spatially as

$$B_{m,n}(x,z) = \frac{ikz}{2\pi} \int_{-\infty}^{\infty} w(x' - mL) e^{in\Omega x} \frac{H_1^{(1)}(kR)}{R} dx' \tag{76}$$

3.2 Gabor Expansion Evaluation

The formulation for one dimensional aperture developed in the previous section is evaluated numerically. The expansion coefficients in (24) are simplified as

$$\mathbf{A}_{m,n} = \int_{-L_0/2}^{L_0/2} \mathbf{f}_t(x)\gamma^*(x - mL)e^{-in\Omega x}dx \tag{77}$$

where aperture distribution $\mathbf{f}(x) = \widehat{y}f(x)$ and the biorthogonal Gamma function is

$$\gamma(x) = \sqrt{\frac{\pi^3}{\sqrt{2}LK_0^3}}e^{\pi(\frac{x^2}{L^2})} \sum_{i \geq \frac{x}{L} - \frac{1}{2}}^{\infty} (-1)^i e^{-\pi(i+\frac{1}{2})^2} \tag{78}$$

Expansion functions $B_{m,n}(x, z)$ can be evaluated [5] by their saddle-point contribution and subsequently paraxial and far field approximations can be determined.

Simplifying the mapping given in (46) results in

$$x - mL = \rho \sin\Theta \tag{79.a}$$

$$z = \rho \cos\Theta \tag{79.b}$$

$$\boldsymbol{\rho} = \hat{x}(x - mL) + \hat{z}z \tag{79.c}$$

$$\sin\Theta_n = \frac{n\Omega}{k} \equiv \frac{n\lambda}{L} \tag{79.d}$$

$$\Theta = \Theta_t + \Theta_n \tag{79.e}$$

Paraxially approximated saddle point contribution for $B_{m,n}$ is

$$B_{m,n} \sim \sqrt{\frac{-i\sqrt{2}a_n}{L(z_t - ia_n)}} e^{ik(z_t + \frac{x_t^2}{2(z_t - ia_n)})} \tag{80}$$

where

$$x_t = \rho \sin(\Theta - \Theta_n) \tag{81.a}$$

$$z_t = \rho \cos(\Theta - \Theta_n) \tag{81.b}$$

$$a_n = \frac{L^2 \cos^2 \Theta_n}{\lambda} \tag{81.c}$$

and saddle point contribution for the far field approximation yields

$$B_{m,n} \sim \frac{1}{\sqrt{\lambda r}} H_{m,n}(k \sin \Theta) \cos \Theta e^{i(kr - \frac{\pi}{4})} \tag{82}$$

here $H_{m,n}$ is the Fourier transform of the elementary window function (71) in a coordinate system defined by mapping in (79)

$$H_{m,n}(k \sin \Theta) = \sqrt{\frac{\sqrt{2}2\pi}{\Omega}} e^{-\pi \frac{k^2 (\sin \Theta - \sin \Theta_n)^2}{\Omega^2}} e^{-imLk \sin \Theta} \tag{83}$$

3.3 Numerical Results for One Dimensional Aperture

The formulation developed in previous sections for one dimensional aperture is evaluated numerically. A computer code has been developed and was used to obtain numerical results for pulsed and tapered aperture distributions. Gamma function $\gamma(x)$ was determined numerically as shown on Figure 3 in one dimensions. Comparison of obtained numerical results for $\gamma(x)$ with previously published work [3] showed

good agreement. The aperture fields considered in numerical evaluation are pulsed and cosine distributions shown in Figure 4. The variable chosen in numerical evaluation is the width of the beam waist (L) relative to the width of the aperture (L_0). The Gabor coefficients are determined from (77) with simple numerical integration. The magnitudes of these coefficients are plotted for various values of L_0/L in Fig 5.

3.3.1 Uniform Aperture Distribution

One possible way to check the validity for the choice of the relative beam width and corresponding number of the expansion coefficients is through the aperture field regeneration using equation (70). As seen in Figure 6(a) the pulsed aperture distribution is given as

$$f_t = \begin{cases} 1, & x \in [-\frac{L_o}{2}, \frac{L_o}{2}] \\ 0, & elsewhere \end{cases} \tag{84}$$

Regeneration with inadequate number of coefficients $-6 \leq n \leq 6$ for the $L_0/L = 0.2$ results in an inaccurate representation. As n increases to include $-19 \leq n \leq 19$ as shown in Figure 6(b), this agreement improves. Further increase in n to include $-49 \leq n \leq 49$ shows better convergence. Similar observations were made for narrower beams in Figure 7, where L_0/L is chosen as 9. However, convergence with less number of terms is achieved sooner for narrower beams. The radiated field patterns from a pulsed aperture (84) using (74) are determined at various observation locations away from the aperture and are shown in Figure 8. At $z = 2.4\lambda$ at the near zone, the pattern shown in Figure 8(a) resembles the aperture distribution itself. As one moves further away from the aperture, the radiated pattern approaches its Fourier transform

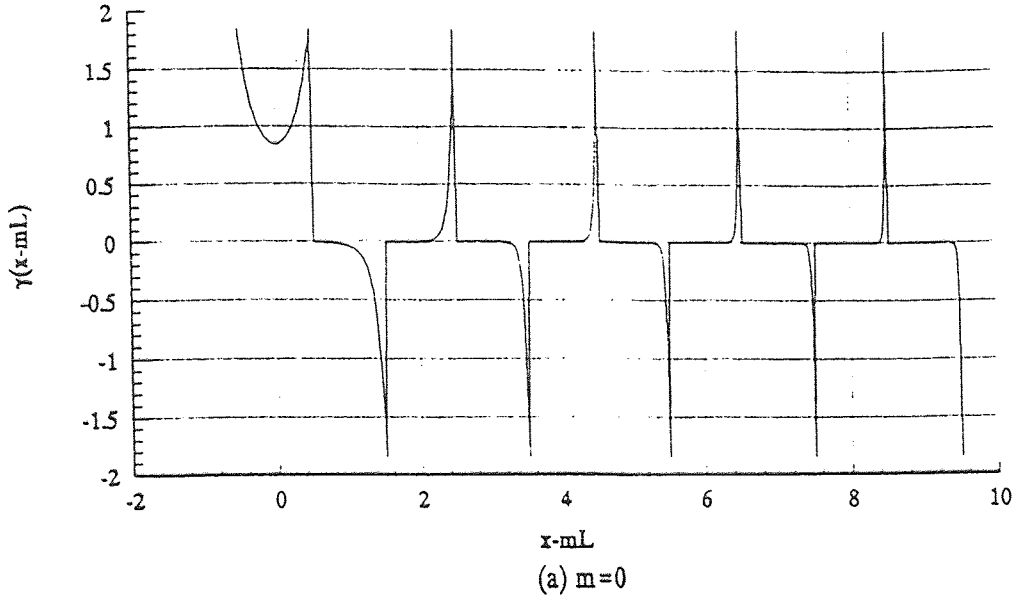

(a) m=0

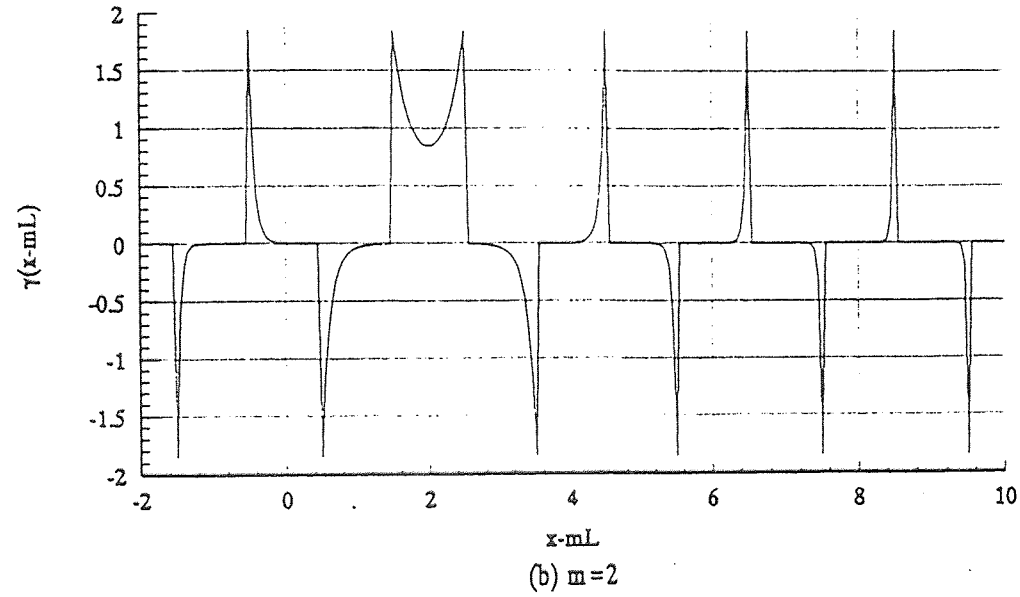

(b) m=2

Figure 3. Gamma function γ(x-mL) versus its argument.

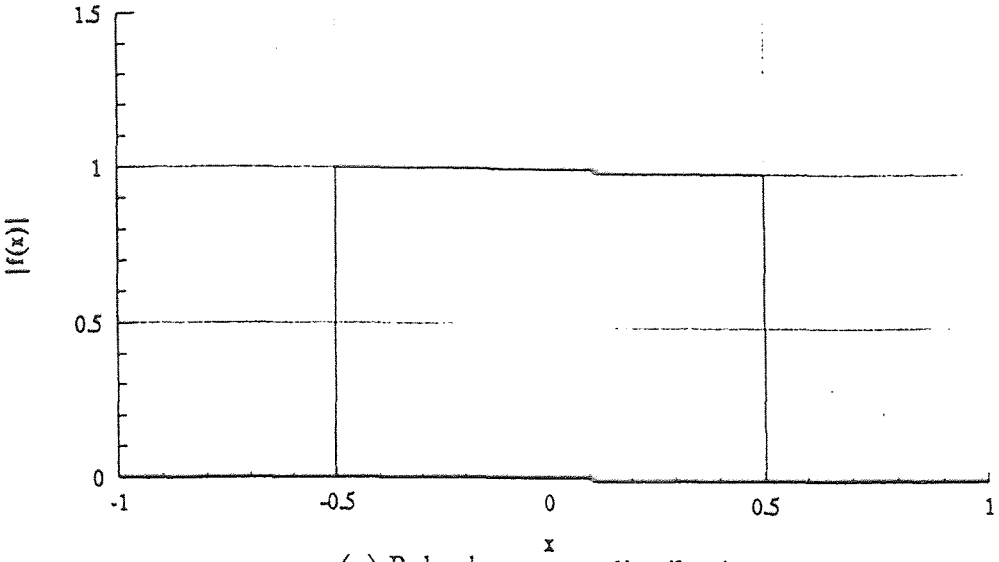

(a) Pulsed aperture distribution

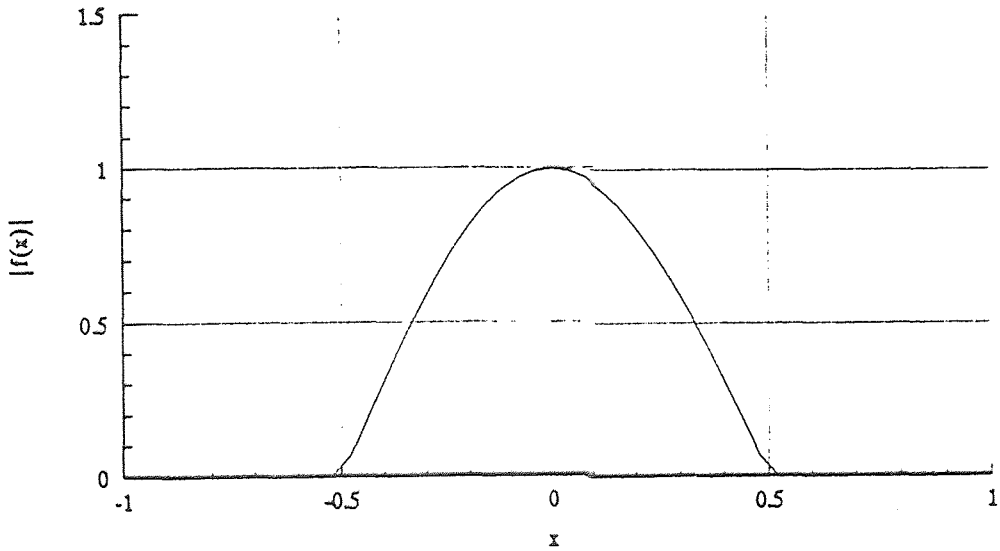

(a) Tapered aperture distribution

Figure 4. Pulsed and tapered (cosine) aperture field distributions.

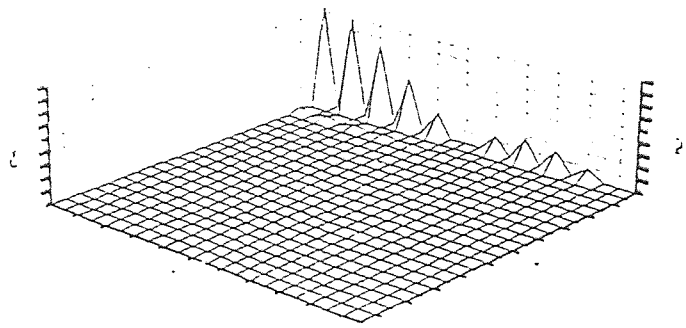

(a) $L_0/L = 0.2$

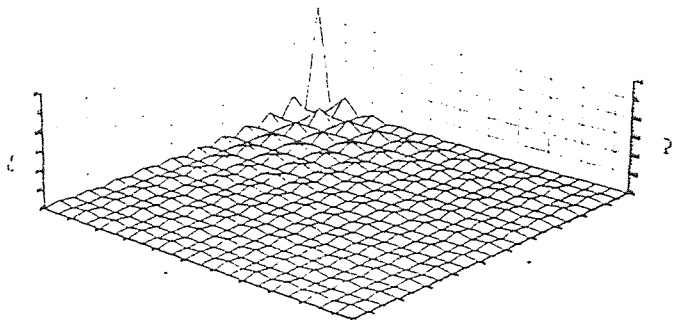

(b) $L_0/L = 1.0$

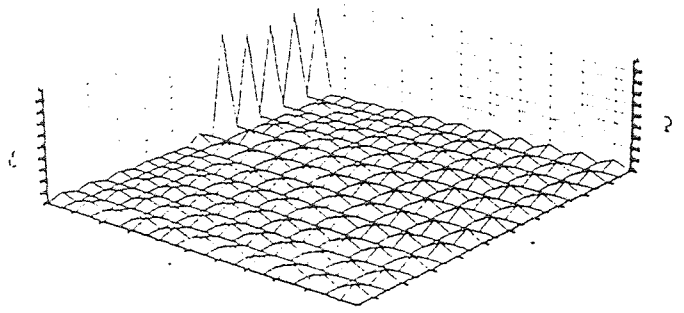

(c) $L_0/L = 9.0$

Figure 5. Expansion coefficients $|A_{mn}|$ for a pulsed aperture for various values of L_0/L.

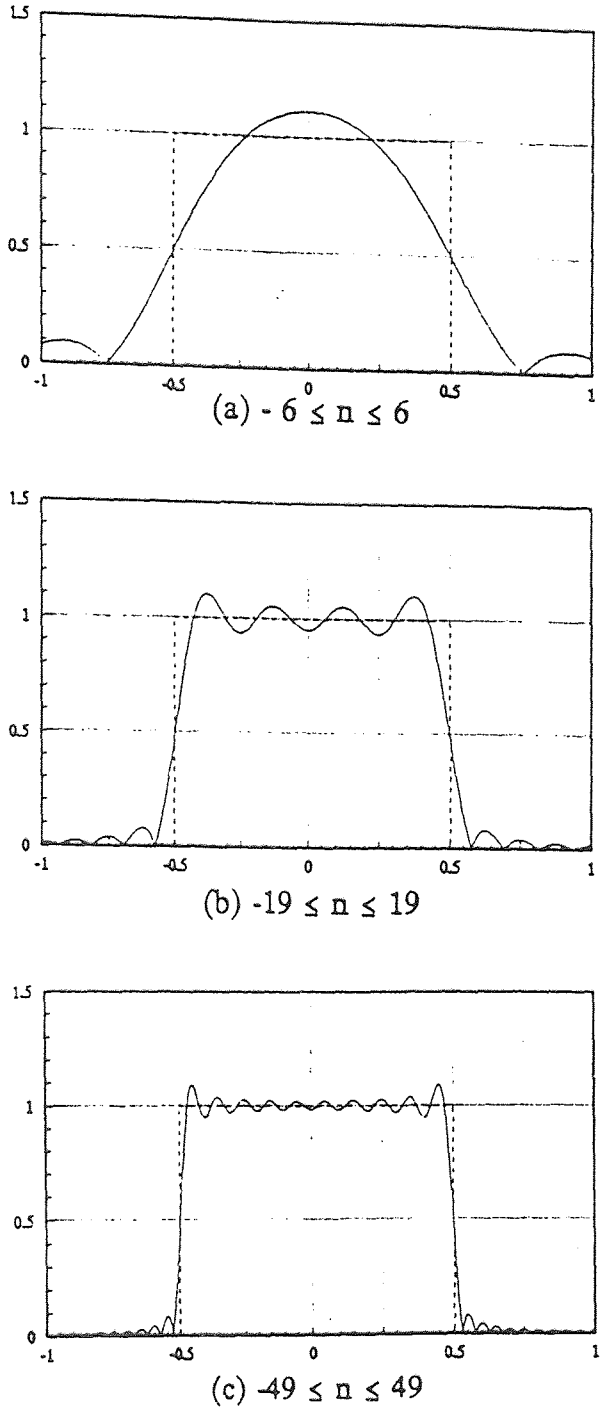

Figure 6. A Gabor representation (— solid line) of a pulsed aperture (– – dashed line) with $L_0/L=0.2$ and $-9 \leq m \leq 9$ and various values versus n.

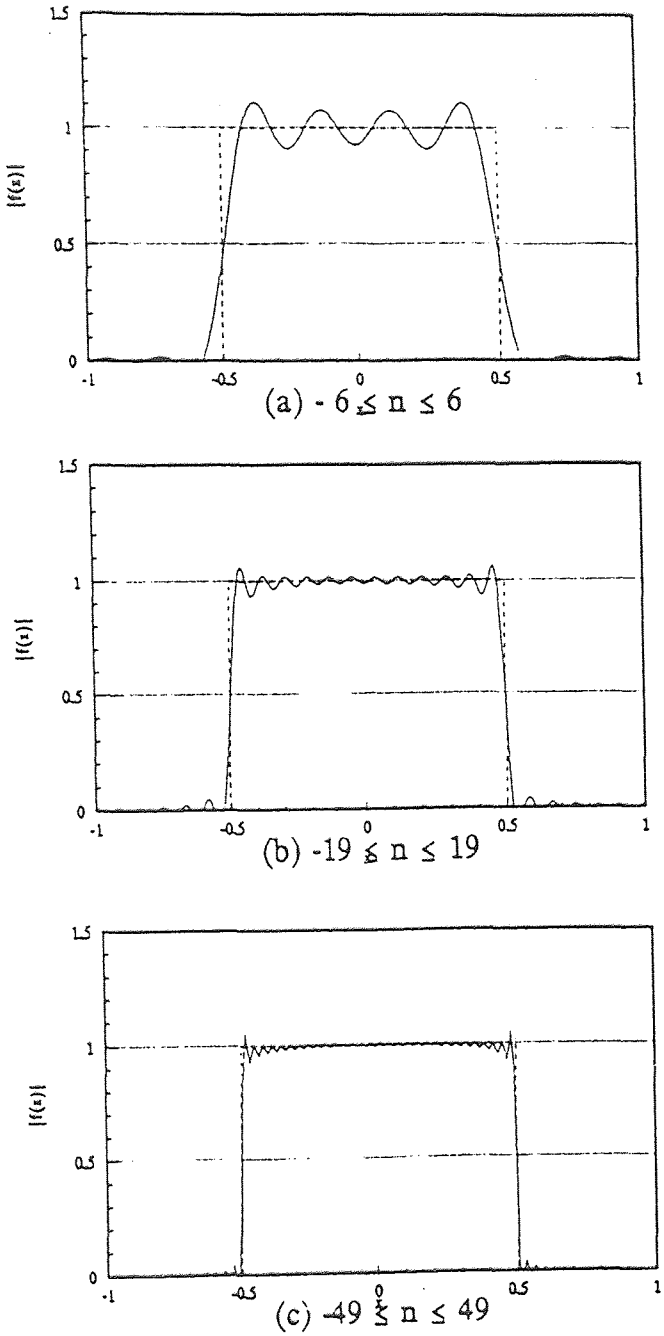

Figure 7. A Gabor representation (— solid line) of a pulsed aperture (– – dashed line) with L_0/L=9.0, -9 ≤ m ≤ 9 and various values versus n.

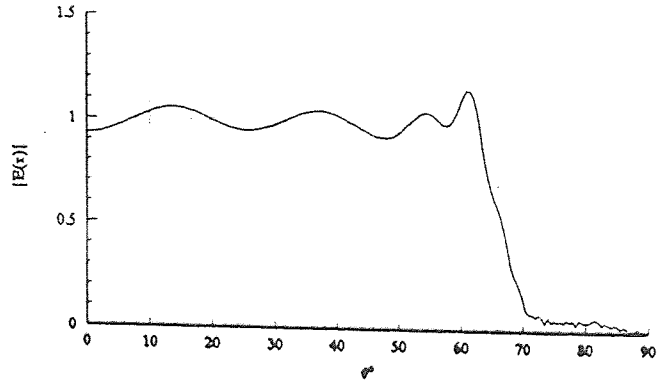

(a) $z = 2.4\lambda$

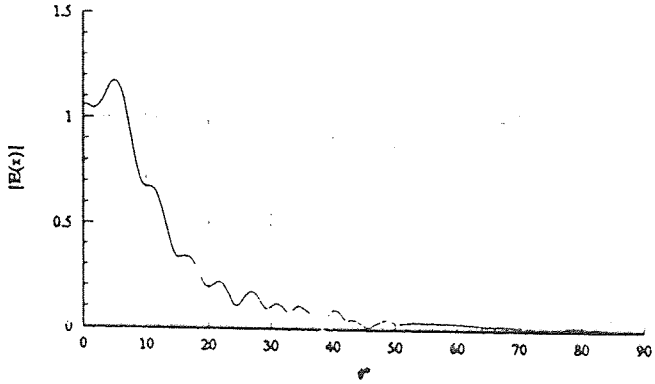

(b) $z = 24\lambda$

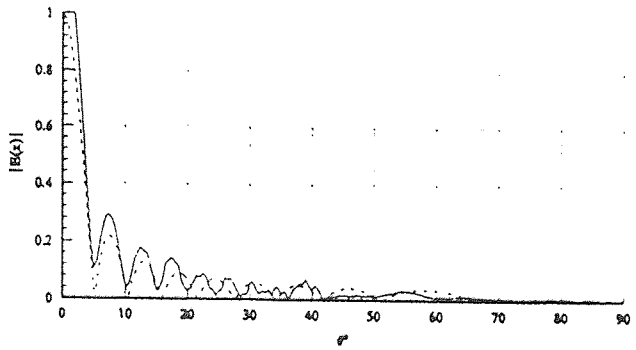

(c) $z = 240\lambda$

Figure 8. Far field distribution of a pulsed aperture for various values of observation point z.
(— solid line) Gabor representation $-9 \le m \le 9$, $-11 \le n \le 11$,
in (c) the theoretical far field expression (– – dashed line) was obtained from a Fourier Transform of an aperture field.

in the form of $\left|\frac{\sin(x)}{x}\right|$. All these numerical results are in good agreement with those published previously [5]-[6].

3.3.2 Tapered Aperture Distribution

More typical aperture illumination in practice created by wave guide feeds is tapered in amplitude variation. Cosine field distribution along the aperture

$$f_t = \begin{cases} \cos(\frac{\pi x}{L_o}), & x \in [-\frac{L_o}{2}, \frac{L_o}{2}] \\ 0, & elsewhere \end{cases} \tag{85}$$

as shown in Figure 4(b) is considered next. The Gabor expansion coefficients are given in Table 1 for $L_0/L = 9$. Only significant coefficients are retained in the table.

The aperture field re-generation is shown on Figure 9 and good agreement was observed with very small number of terms. One reason for rapid convergence is that Gaussian beam expansion functions are indeed a good choice for tapered aperture representation. This is evident in Figure 6(a) where a pulsed aperture was attempted to be represented by a few terms but a tapered approximate distribution was achieved. Similar trend is observed for far field evaluation from a tapered distribution as seen in Figure 10. Here, as observation location is removed further away from the aperture, the field pattern changed from almost aperture distribution itself into the theoretical value of the far field. All these evaluations verified that the numerical code developed produces reliable results which are accurate in comparison to the ones previously published[5-6]. In general, one can conclude that narrow beams adequately can be utilized to analyze and synthesize the radiated field from the aperture.

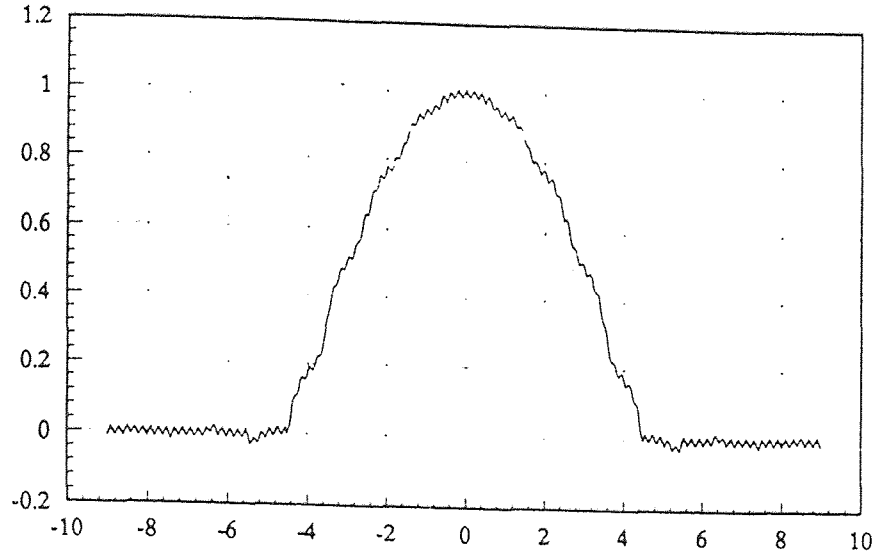

(a) $|M| \leq 9$ $|n| \leq 6$

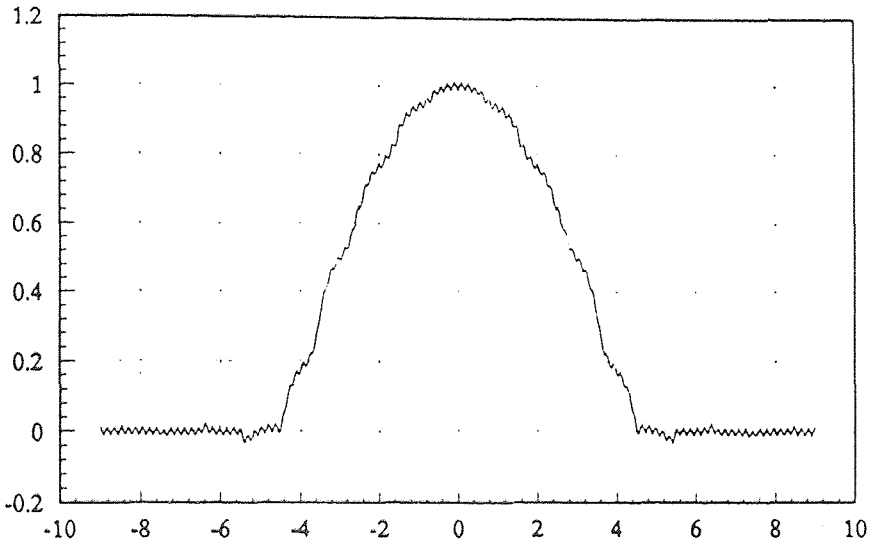

(b) $|M| \leq 9$ $|n| \leq 49$

Figure 9. A Gabor representation (— solid line) of a tapered cosine aperture distribution for $L_0/L=9.0$, $-9 \leq m \leq 9$ and various values versus n.

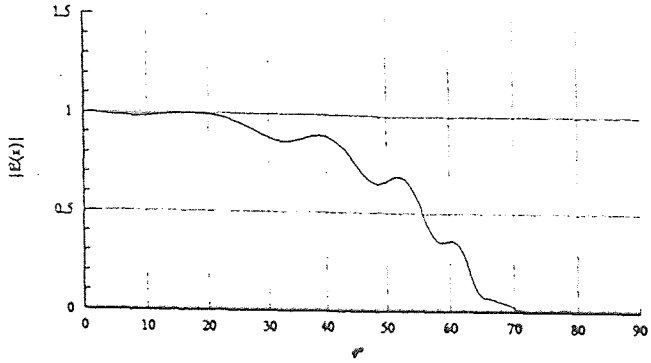

(a) z=2.4λ

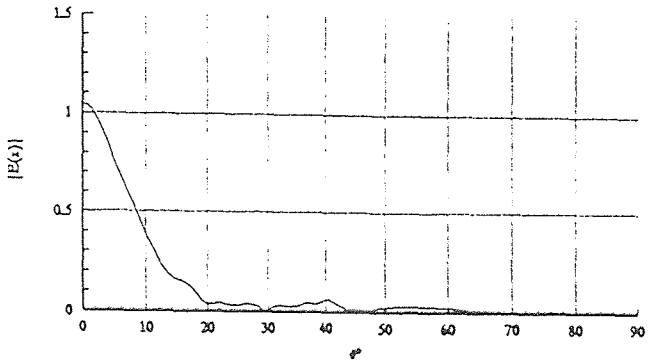

(a) z=24λ

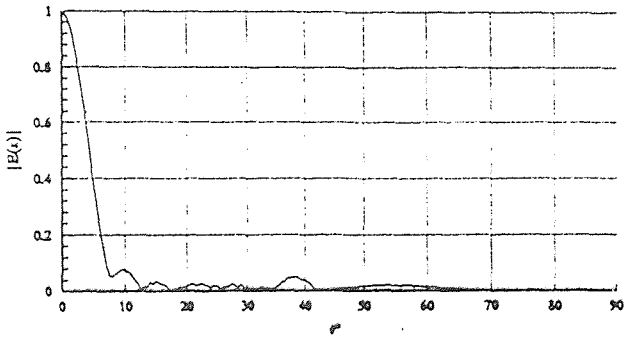

(c) z=240λ

Figure 10. Far field distribution of a cosine aperture for various values of observation point z.
(— solid line) Gabor representation $-9 \le m \le 9, -11 \le n \le 11$.

```
   M=0
N=0 (0.797524263112485,0.0)
N=1 (1.521202323052012E-002,9.292967870916380E-017)
N=2 (-5.144546963027078E-002,1.517883041479706E-017)
N=3 (5.221507078496231E-002,7.372574772901430E-018)
   M=1
N=0 (0.856042996319709,0.0)
N=1 (-9.149063203533468E-002,3.721373120646945E-003)
N=2 (5.540630799088465E-002,7.515160384644251E-004)
N=3 (-5.234122091440698E-002,-1.099984598654556E-003)
   M=2
N=0 (0.596228663687248,0.0)
N=1 (2.569564533161399E-002,1.045802373201928E-002)
N=2 (-5.217146938472059E-002,-3.564178600955657E-003)
N=3 (5.178608044478288E-002,2.552601731278998E-003)
   M=3
N=0 (0.486639099012307,0.0)
N=1 (-7.735957904535368E-002,6.564320514250380E-003)
N=2 (5.452902074869215E-002,4.484187026507899E-003)
N=3 (-5.090817830638630E-002,-4.168217032210447E-003)
   M=4
N=0 (7.518084762507365E-002,0.0)
N=1 (5.346857568579928E-002,2.618901174329920E-002)
N=2 (-5.090733311071495E-002,-1.105695744077676E-002)
N=3 (4.851514517813611E-002,6.108145482827882E-003)
   M=5
N=0 (1.859810992660984E-002,0.0)
N=1 (-3.117363510295848E-002,-1.321360284507505E-002)
N=2 (4.028946513231653E-002,9.796802893705825E-003)
N=3 (-4.320566467744310E-002,-5.893907614704491E-003)
   M=6
N=0 (-3.085734556352576E-002,0.0)
N=1 (3.360249220121488E-002,4.732677394055694E-003)
N=2 (-3.792015356277144E-002,-5.327284442685197E-003)
N=3 (4.075495800875020E-002,3.874121867533754E-003)
```

Table 1. Gabor expansion coefficients for a cosine aperture distribution. The parameters chosen are $-9 \le m \le 9$, $-6 \le n \le 6$ and $L_x/L=9.0$. Only significant coefficients are retained here.

CHAPTER 4

NUMERICAL RESULTS FOR TWO DIMENSIONAL APERTURES

The Gabor expansion in terms of a Gaussian beam representation for the two dimensional aperture field distributions were formulated by Einzinger, et.al. [5] and applied in complicated environments by Maciel [6]. The detailed theory is presented in Chapter 2 of this thesis. In this chapter, numerical results for pulsed and tapered aperture distributions are presented and validity of the current approach is discussed. The numerical evaluation of two dimensional apertures follow very similar steps of one dimensional aperture presented in Chapter 3. Results are presented only for the electric field vector potential $\bar{\psi}(\mathbf{r})$, without any significant loss, but can be extended to fields via differentiation as shown in (62)-(64). Two dimensional Gamma function $\gamma(x - mL_x, y - pL_y)$ in (23) is a product of two one dimensional Gamma functions. Plot of this function is shown in Figure 11. The choice of number of terms to be kept in the expansion was based on aperture re-generation, as was done in Chapter 3. However, further numerical evaluations were based on the fact that narrow beam summation is best suited to synthesize far fields as has been obtained in Chapter 3.

4.1 Uniform Aperture Field Distribution

The uniform aperture distribution in two dimensions can be expressed as

$$f(x,y) = \begin{Bmatrix} 1, & |x| \leq \frac{L_{ox}}{2} \quad and \quad |y| \leq \frac{L_{oy}}{2} \\ 0, & elsewhere \end{Bmatrix} \tag{86}$$

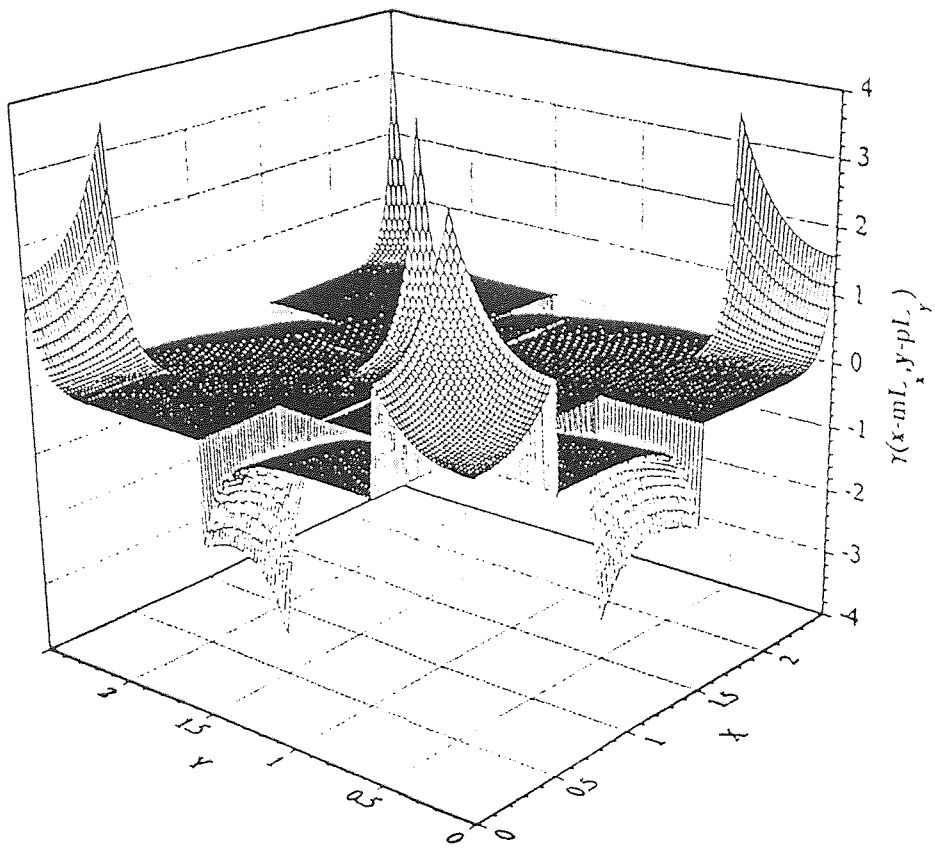

Figure 11 Two dimensional gamma function $\gamma(x\text{-}ml_x, y\text{-}pl_y)$ versus its arguments.

In practice, it is rather difficult to synthesize true pulsed aperture distribution but it is useful for numerical simulations to investigate the merits and limitations of the applied methods.

The Gabor expansion coefficients $A_{m,n,p,q}$ are determined from direct two dimensional numerical integration of (24). Beam widths L_x, L_y, in x and y directions, respectively, are the parameters that can be varied in a Gabor scheme. These coefficients for the pulsed aperture distribution in (86) are shown in Figure 12 for various choices of L_{ox}/L_x and L_{oy}/L_y where L_{ox} and L_{oy} are the aperture dimensions in wavelengths. The choice of $n = q = 0$ excludes so called tilted beams with additional phase factor. Further it will be shown that the wide beams chosen in Figure 12(a) and 12(b) are not suited for consideration due to their lack of convergence. The aperture field re-generation using (12) as shown in Figure 13 and 14 clarifies this aspect. The chosen wide beam widths of $L_{ox}/L_x = L_{oy}/L_y = 0.2$ show rather poor convergence to synthesize a rectangular pulsed aperture distribution. Decreasing beam widths to $L_{ox}/L_x = L_{oy}/L_y = 9.0$ yields much more accurate re-generation of an aperture field distribution as seen in Figure 14. However, Gibbs effects are clearly visible in Figure 14, which can be attributed to [5] the contribution of elementary beams associated with larger n and q. Although these beams are evanescent in the long-wavelength limit, they may propagate in the short-wavelength limit ($n, q \approx \frac{L_{x,y}}{\lambda}$ large).

The Gabor summation in (18) for the potential function will be compared with the conventional Fourier Transform representation (10) in the far zone. Using approximation

$$\frac{e^{ikR}}{R} \sim \frac{e^{ikr}}{r} e^{-ikr\cdot\hat{r}'} \tag{87}$$

formula (10) can be rewritten as

$$\bar{\psi}(\mathbf{r}) = \frac{e^{ikr}}{2\pi r} \iint_{-\infty}^{\infty} \hat{z}\times\mathbf{f}_t(x,y) e^{-ik(x\sin\theta\cos\phi + y\sin\theta\sin\phi)} dxdy \tag{88}$$

Introducing the Fourier transform of the aperture field

$$\overline{\mathcal{F}}(k\sin\theta\cos\phi, k\sin\theta\sin\phi) = \iint_{-\infty}^{\infty} \mathbf{f}_t(x,y) e^{-ik(x\sin\theta\cos\phi + y\sin\theta\sin\phi)} dxdy \tag{89}$$

and considering that

$$\overline{\mathcal{F}} = \hat{x}\mathcal{F}^x + \hat{y}\mathcal{F}^y \tag{90}$$

the vector potential can then be expressed as

$$\bar{\psi}(\mathbf{r}) = \frac{e^{ikr}}{2\pi r} \hat{z}\times\overline{\mathcal{F}}(k\sin\theta\cos\phi, k\sin\theta\sin\phi) \tag{91}$$

Then vector potential will become

$$\bar{\psi}(\mathbf{r}) = \hat{y}\mathcal{F}^x(x,y)\frac{e^{ikr}}{2\pi r} \tag{92}$$

Considering uniform aperture distribution, far zone potential amplitude will reduce into

$$\left|\bar{\psi}(\mathbf{r})\right| = \frac{\sin(0.5kL_{ox}\sin\theta\cos\phi)\sin(0.5kL_{oy}\sin\theta\sin\phi)}{(0.5kL_{ox}\sin\theta\cos\phi)(0.5kL_{oy}\sin\theta\sin\phi)} \frac{L_{ox}L_{oy}}{2\pi r} \tag{93}$$

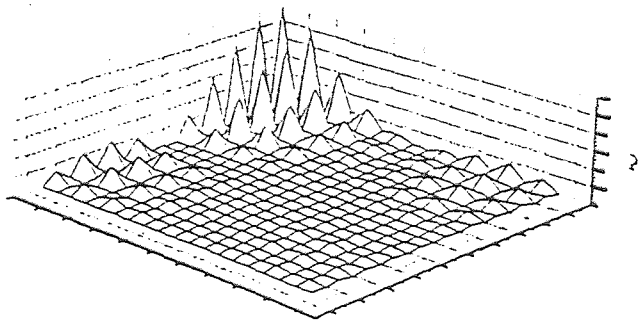

(a) $L_{ox}/L_x = L_{oy}/L_y = 0.2$

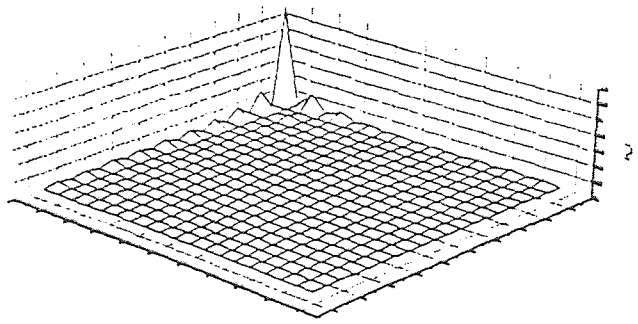

(b) $L_{ox}/L_x = L_{oy}/L_y = 1.0$

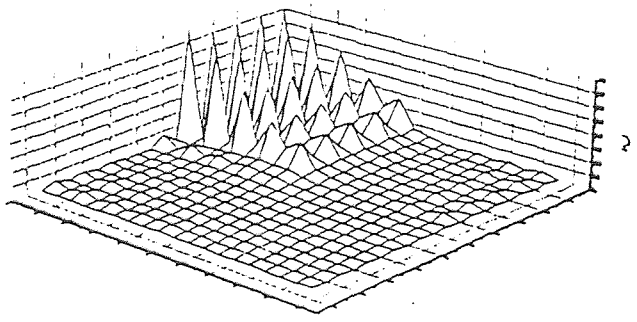

(c) $L_{ox}/L_x = L_{oy}/L_y = 9.0$

Figure 12. Gabor coefficients $|A_{m,n,p,q}|$ of the pulsed aperture for n=q=0 versus m and p.

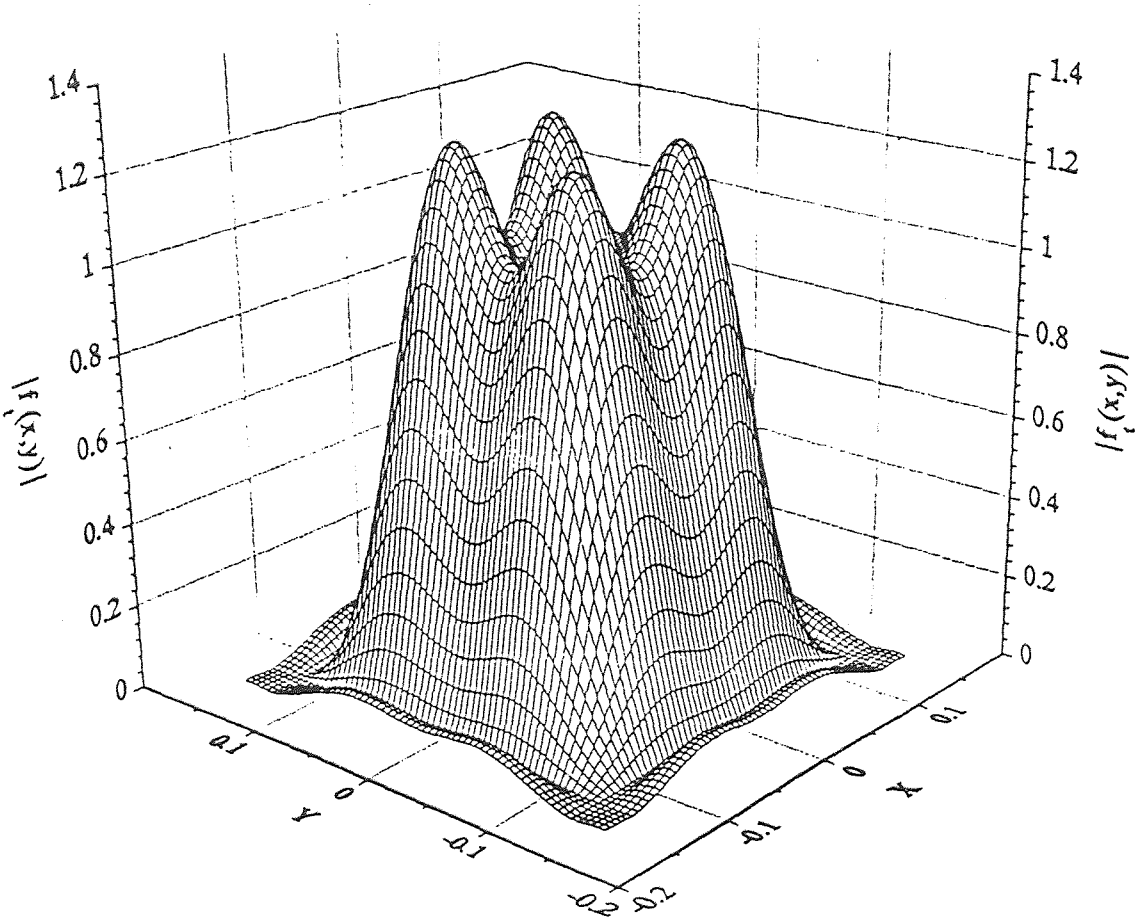

Figure 13. A Gabor representation of a pulsed two dimensional aperture distribution $L_0/L = 0.2$ for $|m|, |n|, |p|, |q| \leq 9$

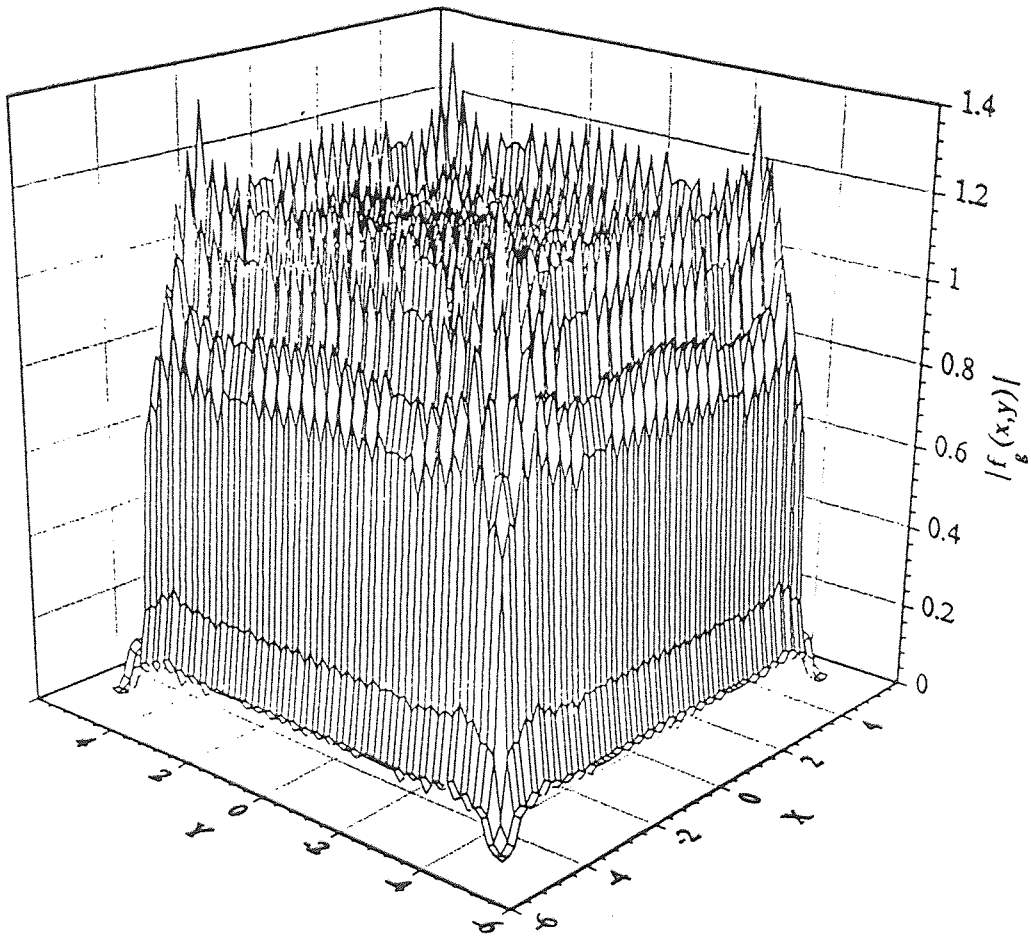

Figure 14. A Gabor representation of a pulsed two dimensional aperture distribution $L_0/L = 9.0$ for $|m|, |n|, |p|, |q| \leq 9$

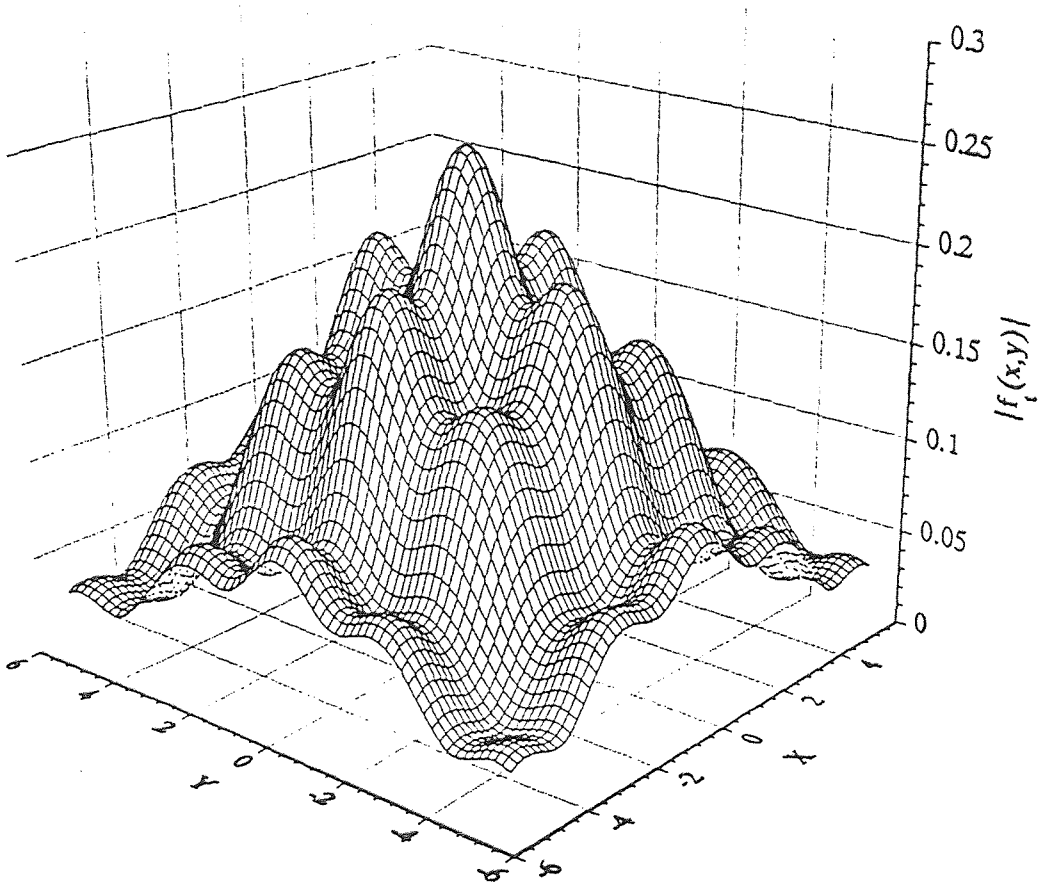

Figure 15. Potential Distribution due toa pulsed aperture in the near zone $z=10\lambda$ for $L_{ox}/L_x = L_{oy}/L_y = 9.0$ and $|m|, |p| \leq 9$ $|n|, |q| = 0$.

Gabor summation in(18) for the pulsed aperture distribution using narrow beams of $L_{ox}/L_x = L_{oy}/L_y = 9.0$ and keeping $n = q = 0$, $|m|$, $|p| \leq 9$ at near field $z = 10\lambda$ is shown in the Figure 15. This potential distribution clearly shows the transition from the aperture field in Figure 14. Further Gabor evaluation at the far zone $z = 100\lambda$ for the same parameters, depicts the typical features of the far field as seen in Figure 16(a). For the comparison, a Fourier Transform for the same pulse aperture distribution is illustrated in Figure 16(b). Comparing both methods based on Figure 16, the Gabor summation could not produce very sharp nulls adjacent to the main lobe. One reason for this inaccuracy could be that $B_{m,n,p,q}$expansion functions were evaluated asymptotically rather than more rigorously using numerical integration. Figure 17 is a replica of Figure 16 using the conventional notation in decibels which helps to reduce the affects of high contrast between the main beam and the side lobes.

4.2 Tapered Aperture Field Distribution.

In general physical apertures, i.e. horn antennas, open ended waveguides, etc., are bounded by metallic enclosures. Tangential electric field components vanish along the exterior boundaries leading to tapered aperture distributions. A cosine field distribution along the two-dimensional rectangular aperture of comparable dimensions can be expressed as

$$f(x,y) = \begin{Bmatrix} \cos(\frac{\pi x}{L0_x})\cos(\frac{\pi y}{L0_y}), & |x| \leq \frac{L0_x}{2} \;\&\; |y| \leq \frac{L0y}{2} \\ 0, & elsewhere \end{Bmatrix} \tag{94}$$

The above aperture field distribution using Gabor representation (14) is regenerated for the rectangular aperture of dimensions $L_{ox} = 5\lambda$ and $L_{oy} = 3\lambda$. The Gabor coefficients are listed in Table 1 and the re-generated aperture field is shown in Figure 18 (a) where Gabor expansion parameters are $L_{ox}/L_x = 10.0$, $L_{oy}/L_y = 6.0$ and $|m|, |n|, |p|, |q| \leq 9$. Comparison of Figure 18(a) with Figure 18 (b) where aperture field distribution (94) is plotted suggests that the above choice of narrow beams and their corresponding number provides good agreement.

Electric field potential (18) that can be used to determine radiated fields was evaluated in the near ($z = 2.0\lambda$), mid ($z = 25\lambda$) and far ($z = 100\lambda$) zones as shown in Figure 19. The radiation patterns were determined for $\phi = 0$ and $\phi = \pi/2$ planes for different values of an angle θ. The far zone patterns in Figures 19 (e) and 19 (f) are compared with the analytical expressions determined using Fourier transform. The far field analytical expression for the two dimensional cosine aperture field distribution can be determined from (89) as

$$\psi(r) = \frac{\cos(0.5kL_{ox}\sin\theta\cos\phi) - i\sin(0.5kL_{ox}\sin\theta\cos\phi)}{(\pi/2)^2 - (0.5kL_{ox}\sin\theta\cos\phi)^2} \times$$

$$\times \frac{\cos(0.5kL_{oy}\sin\theta\sin\phi) - i\sin(0.5kL_{oy}\sin\theta\sin\phi)}{(\pi/2)^2 - (0.5kL_{oy}\sin\theta\sin\phi)^2} \cdot \frac{\pi^2 L_{oy}L_{ox}}{16}\frac{e^{ikr}}{2\pi r} \qquad (95)$$

The comparisons for near and mid zones could be obtained by evaluating Fourier transform numerically. Again the choice of narrow beams in the Gabor expansion confirmed that accurate and reliable representation is possible.

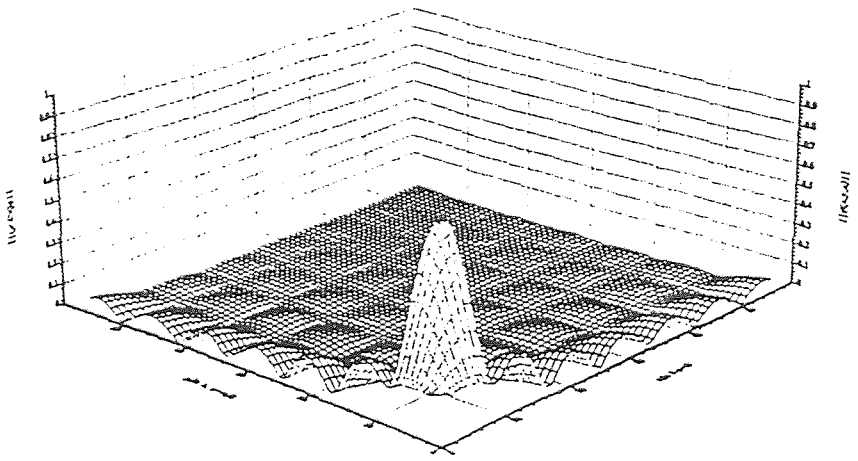

(a)

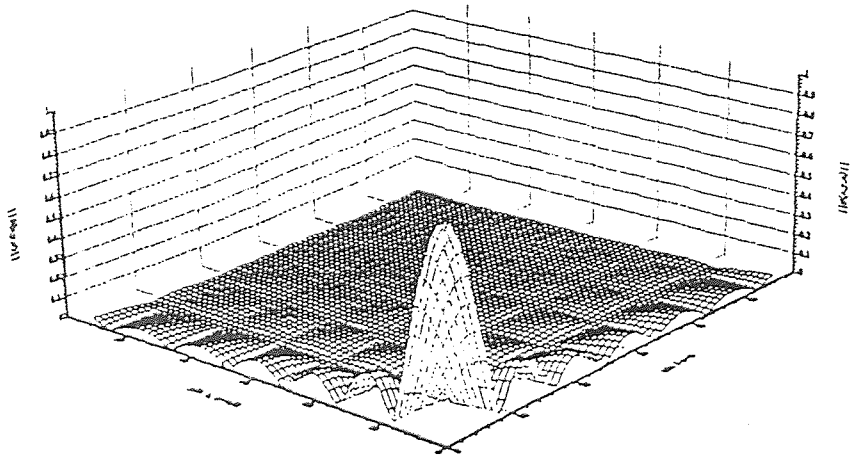

(b)

Figure 16. Potential distribution of the pulsed aperture in the far zone $z=100\lambda$
(a) Gabor summation for $L_{ox}/L_x = L_{oy}/L_y = 9.0$ and $|m|, |p| \leq 9$
(b) Fourier Transform

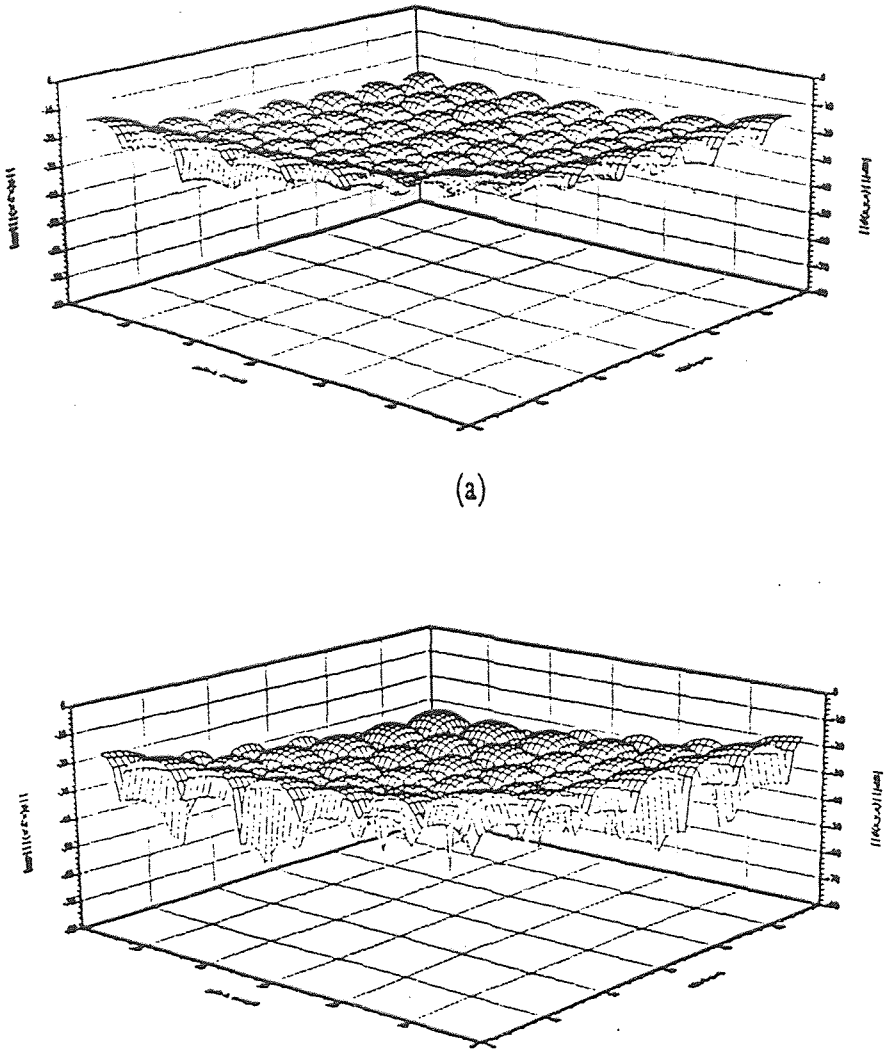

Figure 17. Logarithmic plot of potential distribution of the pulsed aperture in the far zone $z=100\lambda$
(a) Gabor summation for $L_{0x}/L_x = L_{0y}/L_y = 9.0$ and $|m|, |p| \leq 9$
(b) Fourier Transform

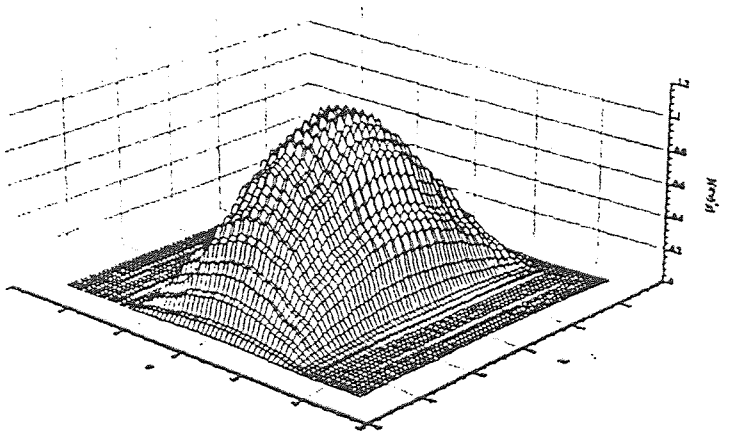

(a)

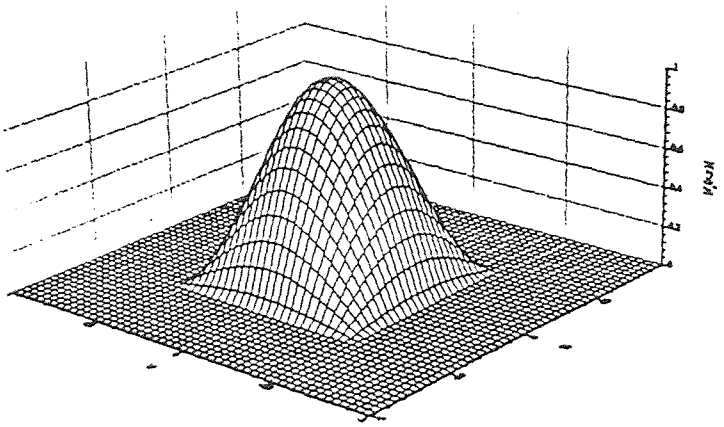

(b)

Figure 18. A Gabor representation of two dimensional cosine aperture distribution $L_{0x}/L_x = 10.0$ $L_{0y}/L_y = 6.0$ for $|m|, |p|, |n|, |q| \leq 9$

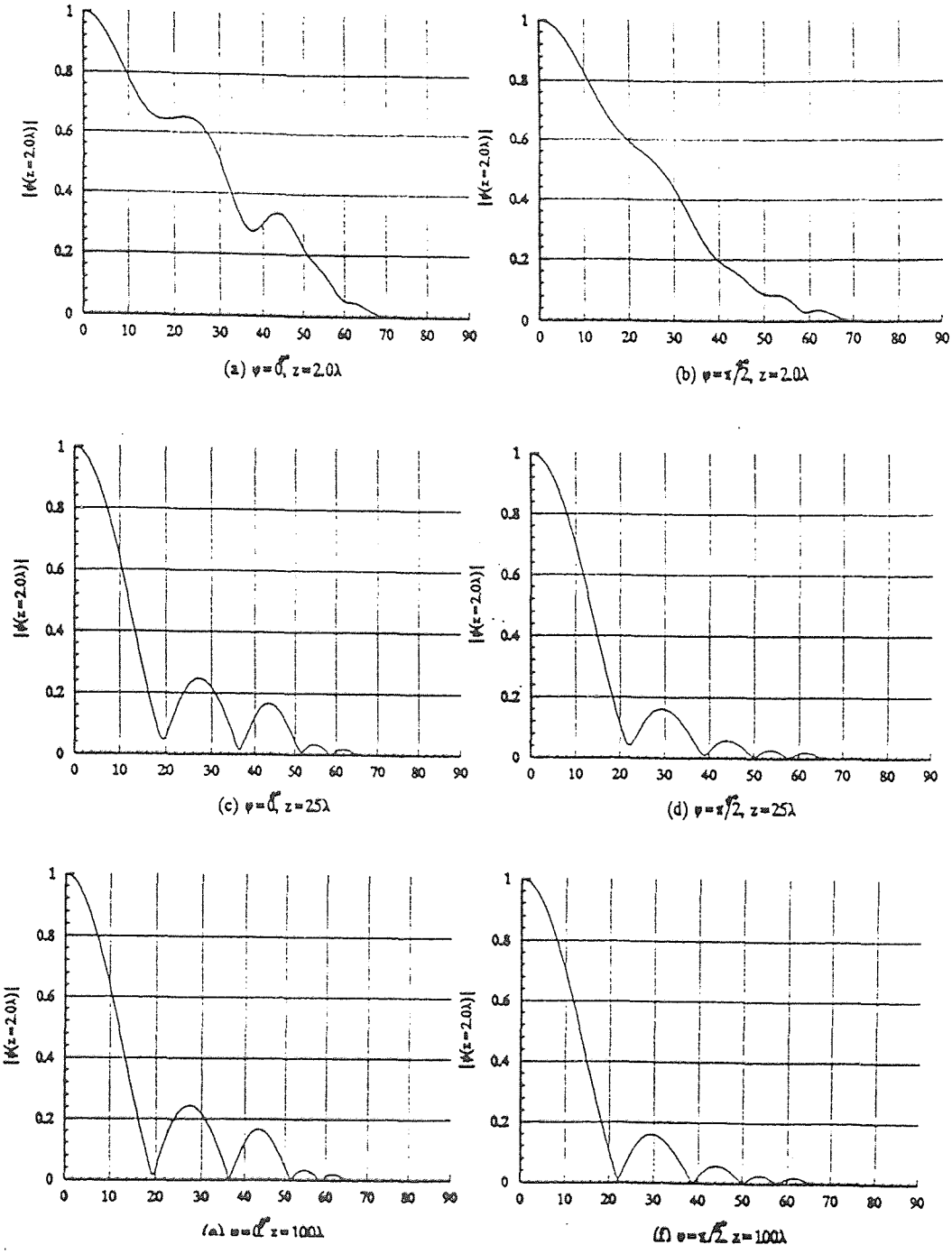

Figure 19. Far field distribution of a cosine aperture for various values of observation point z on $\varphi=0$ and $\varphi=\pi/2$ planes.
Gabor representation parameters are $L_{0x}/L_x = 10.0$ and $L_{0y}/L_y = 6.0$ $|m|, |p| \leq 9$ $|n|, |q|=0$.
Solid lines (—) are obtained by Gabor expantsion and
(– – dashed line) by Fourier Transform (equation(95)).

CHAPTER 5

GABOR REPRESENTATION OF AN EQUIVALENT DIPOLE

The equivalent dipole antenna can be described as a narrow aperture with field distribution similar to the current distribution of an electrical dipole antenna. One major difference between the equivalent dipole and an electrical dipole is that the former radiates only into region $z > 0$ since it is located on $xy-$plane where as a latter one radiates into entire space due to its symmetrical nature. This chapter contains comparisons between rectangular apertures, narrow apertures (one side is much less than the other) and electric dipoles with similar aperture (current) distributions. Similar approach had been reported by Niver [7] where spherical wave expansions have been used compared to the Gabor expansion of the current study.

Though rigorous analysis of determining the radiated fields from a linear, center-fed antenna using Gabor representation has not been done, it is still possible to determine its equivalent solution. This equivalent solution is based on decreasing sufficiently one side of the rectangular aperture while maintaining the aperture distribution similar of a dipole. Thus radiated fields from a narrow aperture will be equivalent to the ones of a dipole in a half space $z > 0$.

5.1 Radiation from a Linear, Center Fed Dipole Antenna

The linear, center-fed dipole antenna as shown in Figure 20 lies along the x-axis and its length is equal to L_{ox}.

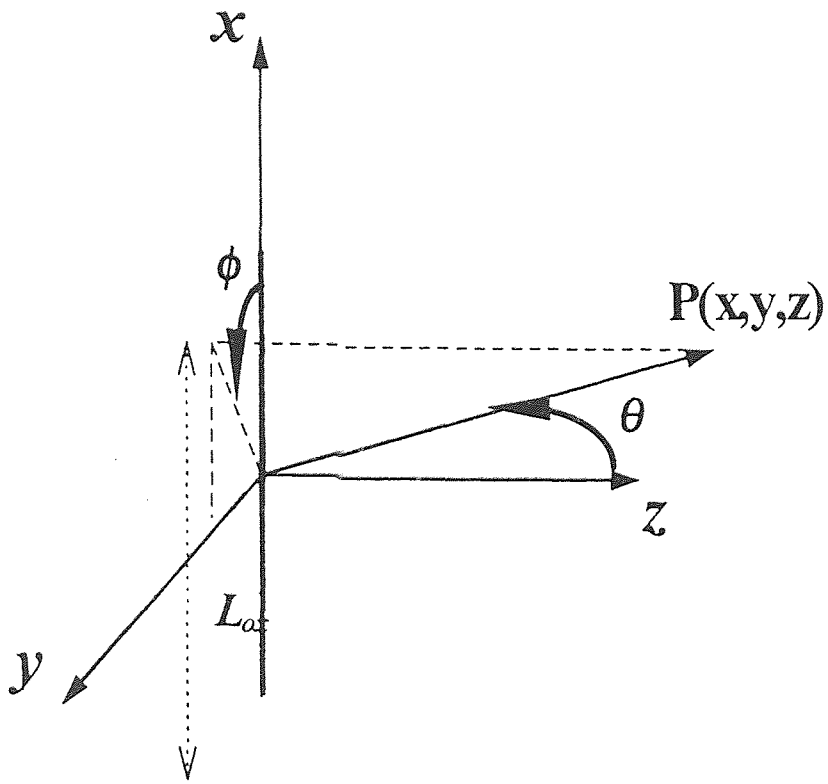

Figure 20. Geometry for a linear, center-fed dipole antenna.

For the sinusoidal current distribution

$$I(x) = I_o \sin(\frac{kL_{ox}}{2} - k\,|x|) \tag{96}$$

The radiation pattern for the linear antenna with current distribution in (96) can be determined as

$$F(\theta,\phi) = \frac{\cos(0.5kL_{ox}\sin\phi\cos\phi) - \cos(0.5kL_{ox})}{1-\sin^2\theta\cos^2\phi} \tag{97}$$

5.2 Radiation from Narrow Apertures

Radiation from two dimensional apertures of comparable dimensions was treated in Chapter 4. Narrow apertures are described as the rectangular aperture where width (L_{oy}) is much smaller than the height (L_{ox}), i.e., $L_{oy} \ll L_{ox}$. Hence, narrow apertures can be viewed as a rectangular aperture $L_{oy}/L_{ox} \ll 1$, in this work this ratio will be taken $L_{oy}/L_{ox} = 0.01$. In order to clarify the transition from the regular aperture ($L_{oy} \sim L_{ox}$) into the narrow aperture ($L_{ox} \gg L_{oy}$), results for both type apertures will be presented.

Various parameters are considered in the numerical experiment to further understand how a transition from a regular aperture into a narrow aperture is applied in terms of Gabor representation. Keeping the aperture field distribution as sinusoidal as shown in figure 21 (a) and 22 (a) Gabor representation involving few terms results in a reasonable re-generated aperture fields as can be seen in Figure 21 (b) and 22 (b) for regular and narrow apertures, respectively. Table 3 and 4 list the Gabor expan-

sion coefficients for square and narrow apertures of Figure 21 and 22, respectively. In above results the height of the considered apertures was kept at $L_{ox} = \lambda/2$. The radiated electric potentials at near, mid and far zones are shown in Figure 23 and 24, where only Gabor expansion coefficients for $n = q = 0$ and $|m|, |p| \leq 5$ were kept. Due to symmetry in excitation $\phi = 0$ and $\phi = \pi/2$ plane patterns in Figure 23 turned out to be identical. But this symmetry disappears for the narrow aperture as seen in Figure 24. However, presence of side lobes suggests that number of the expansion coefficients and choice of beams ($L_x = L_y = 0.05\lambda$) kept in the Gabor representation do not yield accurate results. Changing the beam width to $L_x = L_y = 0.1$ and further to $L_x = L_y = 0.2$ improves convergence a little bit at far field as seen in Figure 25 and 26, respectively. Further increase in the number of terms kept in the Gabor expansion helps to reduce sidelobe levels and give better convergence in spite of presence of Gibbs phenomena near $\theta = \pi/2$. In above Figure 23 through Figure 27 the dashed lines are the theoretical results for the electric dipole.

As can be seen from the above results and comparisons, Gabor representation using wider beams and sufficient number of terms in the expansion is capable of synthesizing the radiation from an electric dipole antenna. However, until present day there has not been any attempt to formulate this problem in a direct approach.

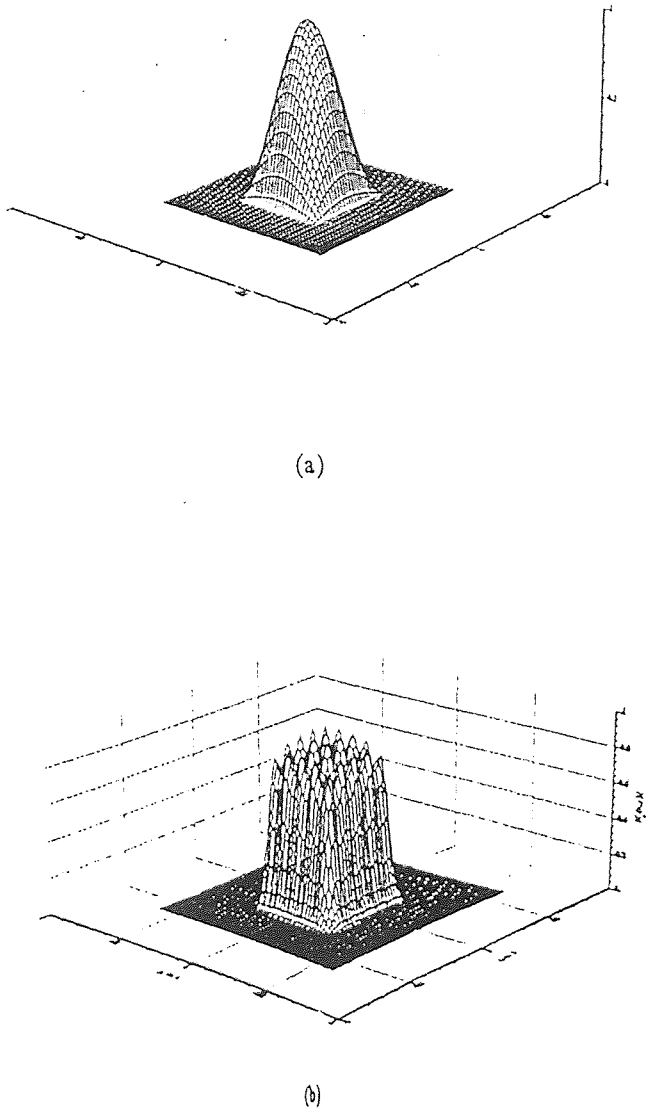

Figure 21 Sinusoidal field distribution of a half-wavelength rectangular aperture ($L_{ox}/L_x=\lambda/2=L_{oy}/L_y=\lambda/2$)
(a) plot of the aperture field
(b) Gabor representation of the aperture field for n=q=0, |m|,|p|≤5.

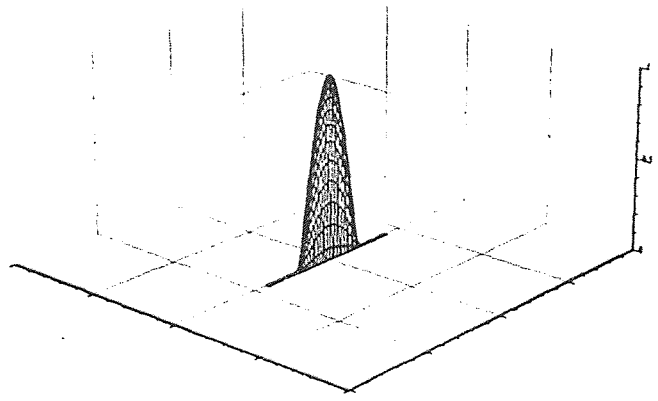

(a)

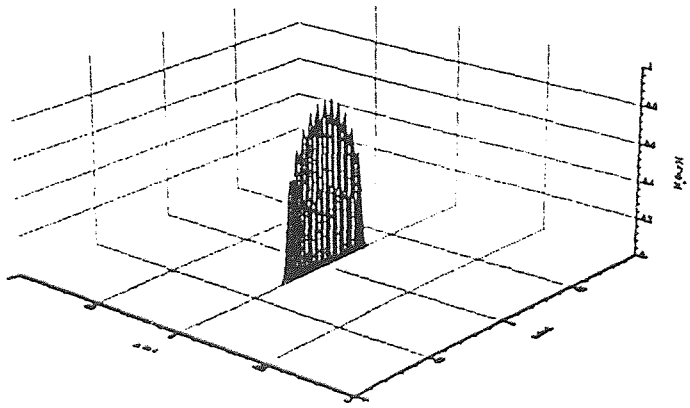

(b)

Figure 22. Sinusoidal field distribution of a narrow half-wavelength rectangular aperture ($L_{0x}= \lambda/2$ $L_{0y}= \lambda/200$)
(a) Plot of the aperture field
(b) Gabor representation of the aperture field for n=q=0, $|m|,|p| \leq 5$.

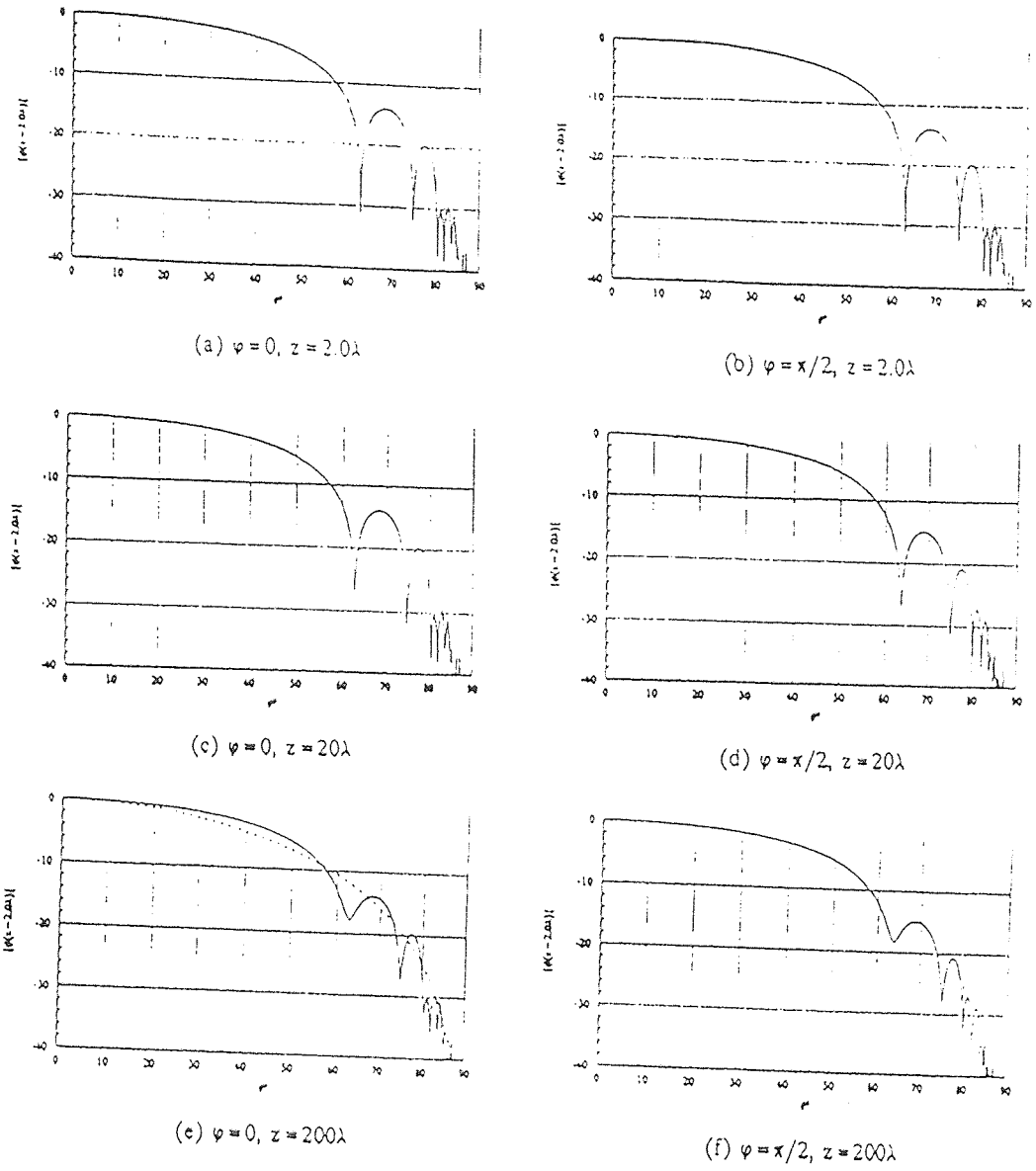

Figure 23 Amplitude of the electric potential of a square aperture ($L_{ox}/L_x=\lambda/2$, $L_{oy}/L_y=\lambda/2$) excited by a sinusoidal field illumination. Gabor parameters are n=q=0, $|m|,|p|\leq 5$
Solid lines (—) are obtained by Gabor expansion and dashed lines (- -) represent theoretical results for an electric dipole.

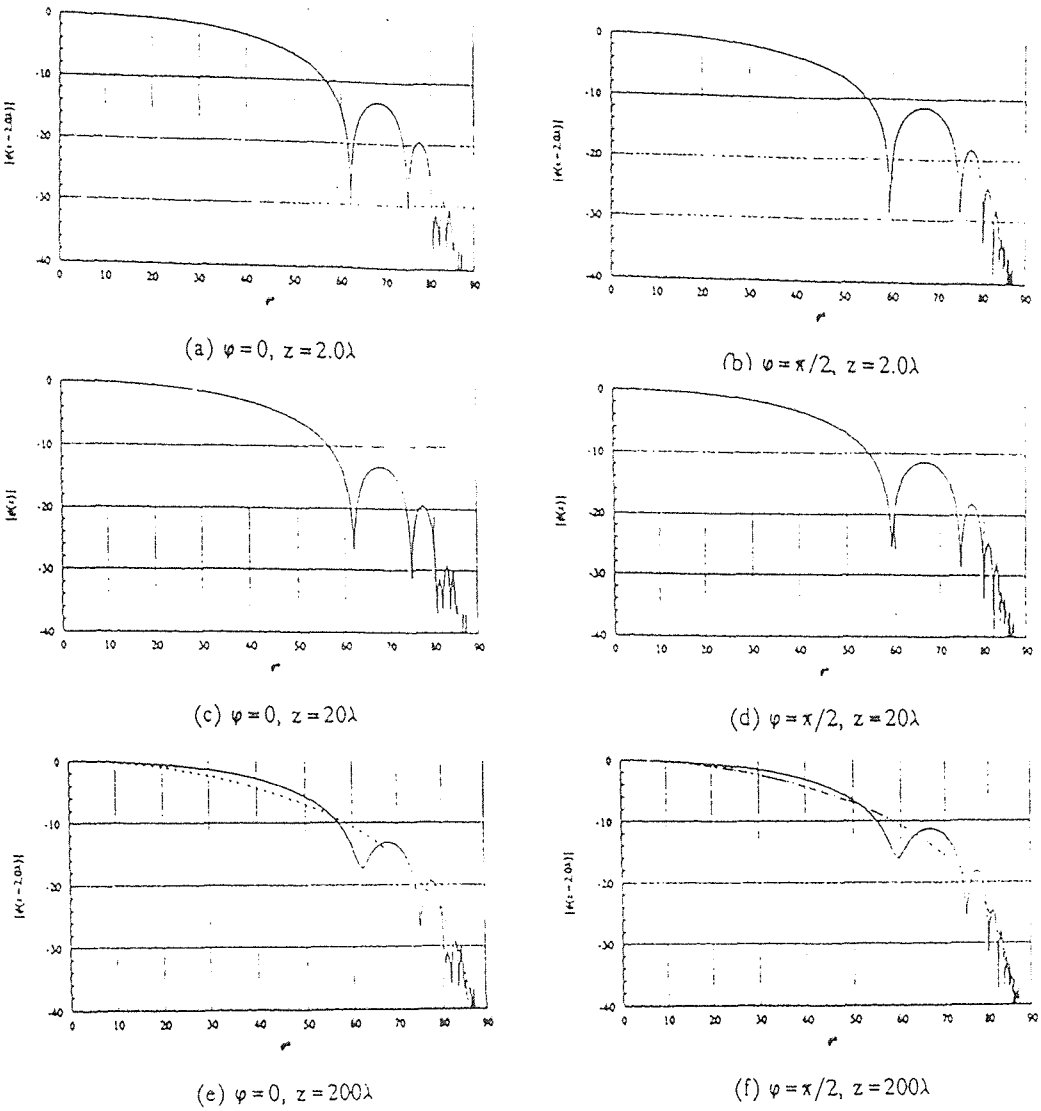

(a) $\varphi = 0$, $z = 2.0\lambda$

(b) $\varphi = \pi/2$, $z = 2.0\lambda$

(c) $\varphi = 0$, $z = 20\lambda$

(d) $\varphi = \pi/2$, $z = 20\lambda$

(e) $\varphi = 0$, $z = 200\lambda$

(f) $\varphi = \pi/2$, $z = 200\lambda$

Figure 24 Amplitude of the electric potential of a narrow aperture ($L_{ox}/L_x=\lambda/2$ $L_{oy}/L_y=\lambda/200$) excited by a sinusoidal field illumination.
Gabor parameters are n=q=0, $|m|,|p| \leq 5$.
Solid lines (—) are obtained by Gabor expansion and dashed lines (- -) represent theoretical results for an electric dipole.

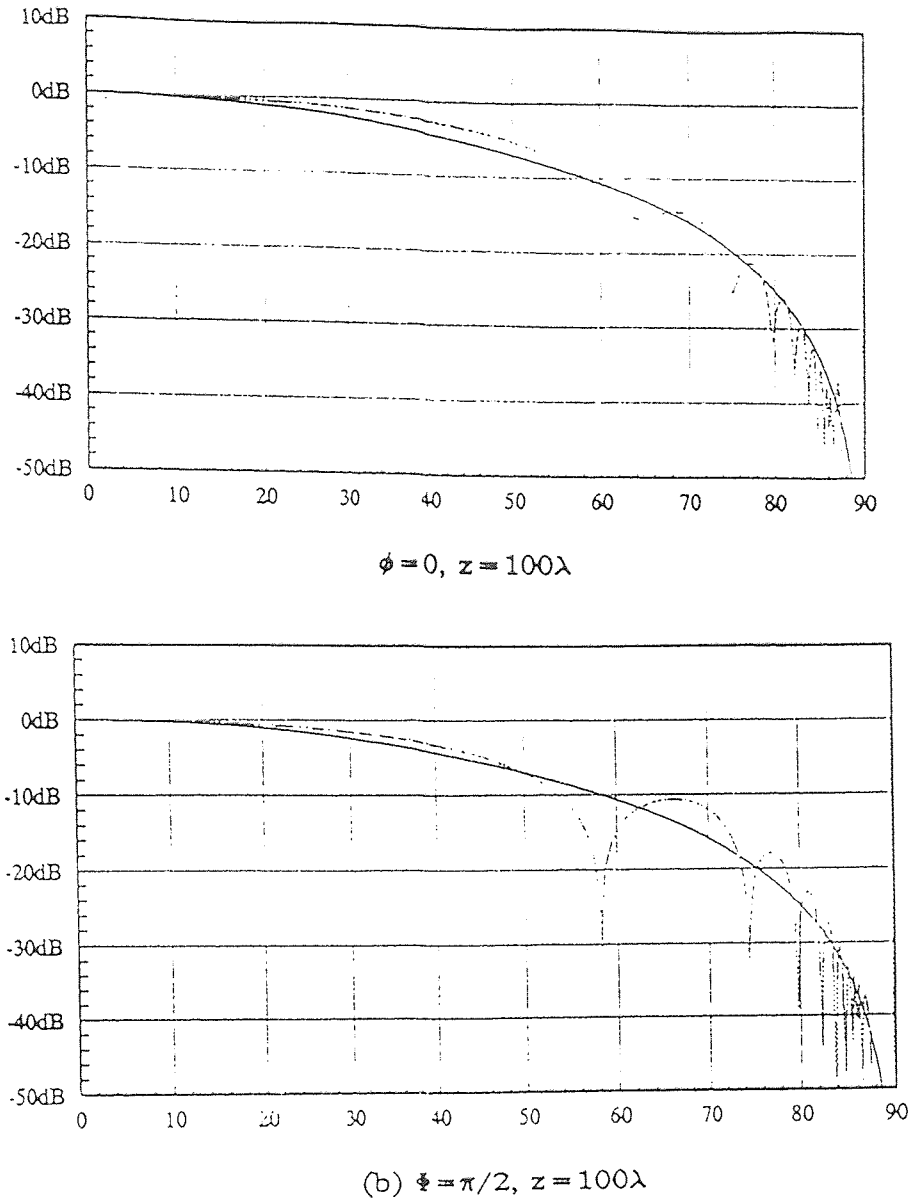

Figure 25 Amplitude of the electric potential of a narrow aperture($L_{ox}/L_x=\lambda/2$ $L_{oy}=\lambda/200$) excited by a sinusoidal field illumination.
Gabor parameters are n=q=0, $|m|,|p| \leq 5$
$L_y=L_x=0.1$
Solid lines (—) are obtained by Gabor expansion and dashed lines (- -) represent theoretical results for an electric dipole.

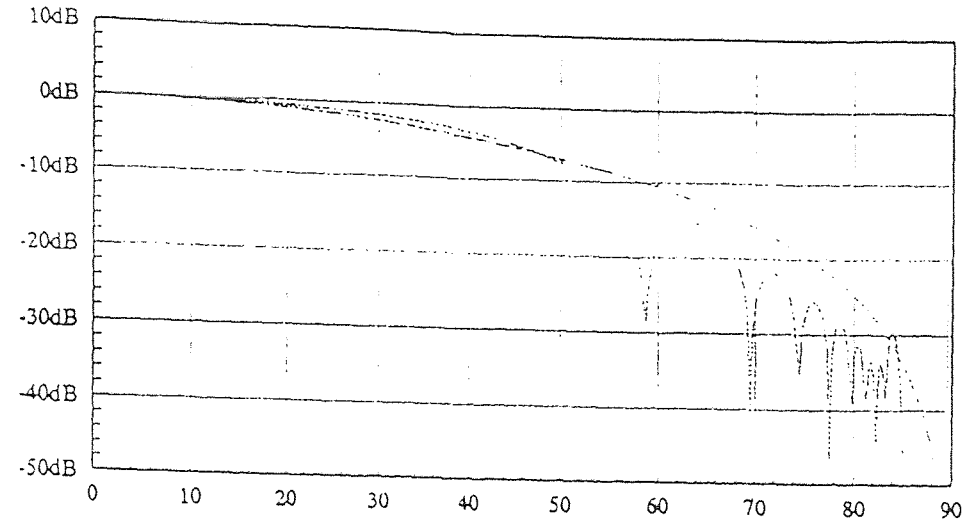

(a) $\Phi = 0,\ z = 100\lambda$

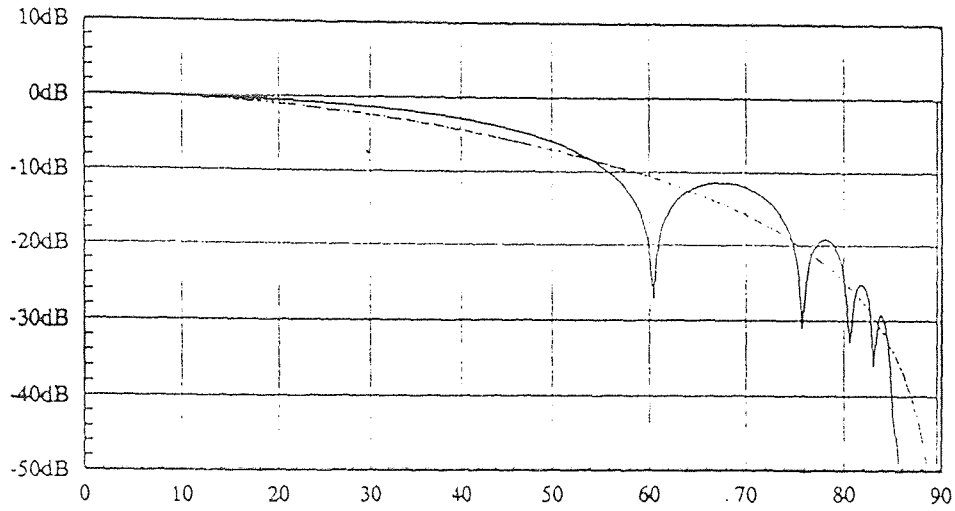

(b) $\Phi = \pi/2,\ z = 100\lambda$

Figure 26 Amplitude of the electric potential of a narrow aperture($L_{ox}/L_x=\lambda/2$ $L_{oy}=\lambda/200$) excited by a sinusoidal field illumination.
Gabor parameters are n=q=0, |m|,|p| ≤ 5
$L_y=L_x=0.2$
Solid lines (—) are obtained by Gabor expansion and dashed lines (- -) represent theoretical results for an electric dipole.

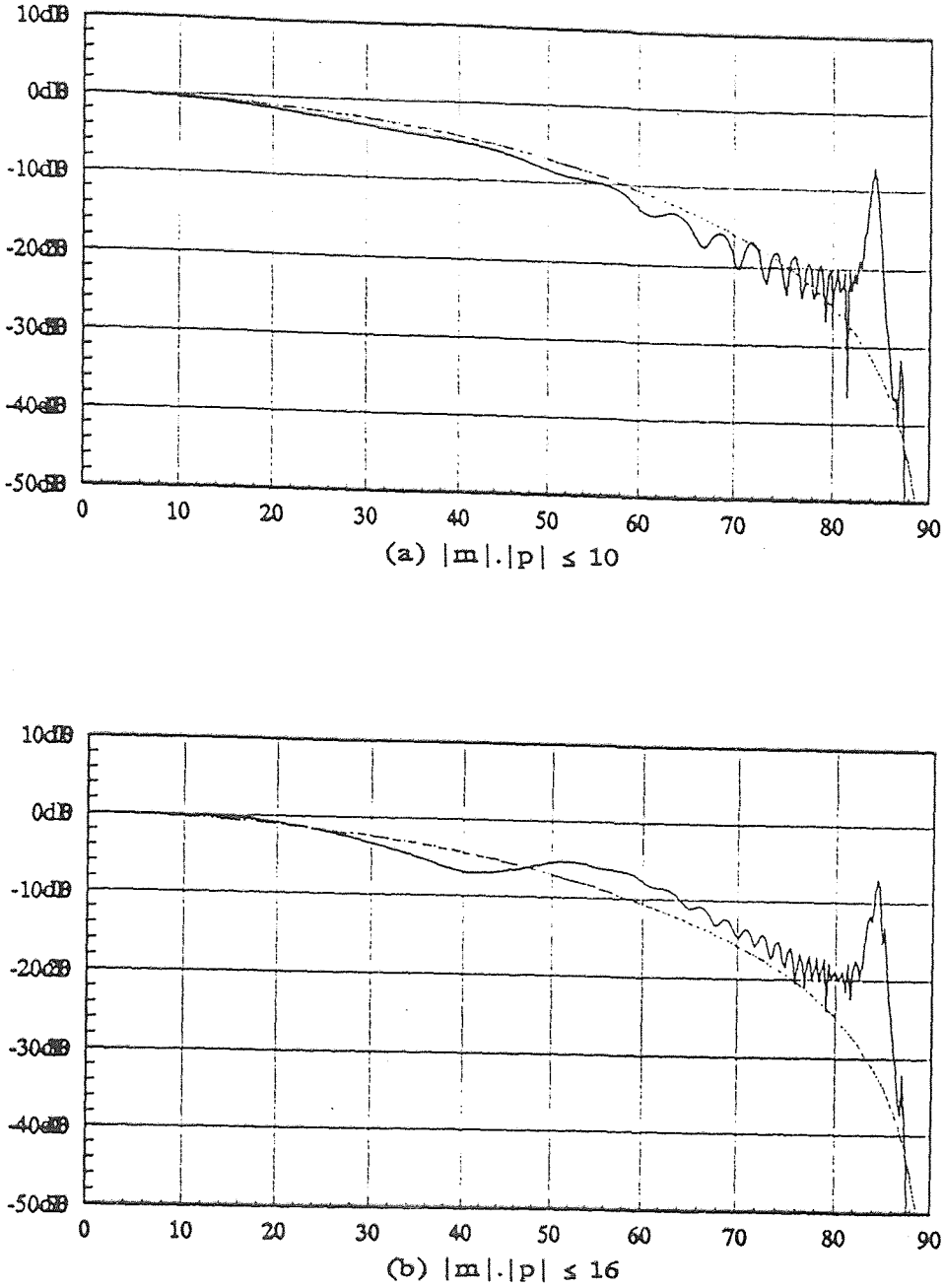

Figure 27. Amplitudes of the electric field potential for the far zone ($z=100\lambda$) of an equivalent half-wavelength dipole at $\varphi=0$ plane.
Gabor parameters are $L_y = L_x = 0.1$ $p=q=0$

	m=0	
p=0		(3.99992547347898,0.0)
p=1		(3.96576525774203,0.0)
p=2		(3.82871337677448,0.0)
p=3		(3.52855128054168,0.0)
p=4		(3.08762119147998,0.0)
p=5		(2.49734279791067,0.0)
	m=1	
p=0		(3.96576525774203,0.0)
p=1		(3.93189677752538,0.0)
p=2		(3.79601534882052,0.0)
p=3		(3.49841670083978,0.0)
p=4		(3.06125224867986,0.0)
p=5		(2.47601495835181,0.0)
	m=2	
p=0		(3.82871337677448,0.0)
p=1		(3.79601534882052,0.0)
p=2		(3.66482981212698,0.0)
p=3		(3.37751580073675,0.0)
p=4		(2.95545920458108,0.0)
p=5		(2.39044698211231,0.0)
	m=3	
p=0		(3.52855128054168,0.0)
p=1		(3.49841670083978,0.0)
p=2		(3.37751580073675,0.0)
p=3		(3.11272653002287,0.0)
p=4		(2.72375817531131,0.0)
p=5		(2.20304157813593,0.0)
	m=4	
p=0		(3.08762119147998,0.0)
p=1		(3.06125224867986,0.0)
p=2		(2.95545920458108,0.0)
p=3		(2.72375817531131,0.0)
p=4		(2.38339556206394,0.0)
p=5		(1.92774805339368,0.0)
	m=5	
p=0		(2.49734279791067,0.0)
p=1		(2.47601495835181,0.0)
p=2		(2.39044698211231,0.0)
p=3		(2.20304157813593,0.0)
p=4		(1.92774805339368,0.0)
p=5		(1.55920931318048,0.0)

Table 2 Gabor expansion coefficients for a rectangular half-wavelength aperture illuminated by sinusoidal field distribution ($L_{ox}/L_x = \lambda/2 = L_{oy}/L_y$) and n=q=0, $|m|,|p| \leq 5$.

	m=0
p=0	(4.192597760148741E-004,0.0)
p=1	(4.326406463615369E-004,0.0)
p=2	(4.754005512573828E-004,0.0)
p=3	(5.562631421993575E-004,0.0)
p=4	(6.930891973502640E-004,0.0)
p=5	(4.576338780666270E-004,0.0)
	m=1
p=0	(4.156792082034351E-004,0.0)
p=1	(4.289458030665117E-004,0.0)
p=2	(4.713405292644499E-004,0.0)
p=3	(5.515125364518168E-004,0.0)
p=4	(6.871700679406246E-004,0.0)
p=5	(4.537255872479741E-004,0.0)
	m=2
p=0	(4.013138553242744E-004,0.0)
p=1	(4.141219732826806E-004,0.0)
p=2	(4.550515908342639E-004,0.0)
p=3	(5.324529538528863E-004,0.0)
p=4	(6.634223309377847E-004,0.0)
p=5	(4.380453991546316E-004,0.0)
	m=3
p=0	(3.698517958261346E-004,0.0)
p=1	(3.816557875528637E-004,0.0)
p=2	(4.193766196474797E-004,0.0)
p=3	(4.907098984068102E-004,0.0)
p=4	(6.114115853045609E-004,0.0)
p=5	(4.037036732753861E-004,0.0)
	m=4
p=0	(3.236348721349447E-004,0.0)
p=1	(3.339638292909560E-004,0.0)
p=2	(3.669710413946484E-004,0.0)
p=3	(4.293904667179063E-004,0.0)
p=4	(5.350091914245700E-004,0.0)
p=5	(3.532565967107164E-004,0.0)
	m=5
p=0	(2.617637226059903E-004,0.0)
p=1	(2.701180333079220E-004,0.0)
p=2	(2.968150658499078E-004,0.0)
p=3	(3.473014087701162E-004,0.0)
p=4	(4.327283912634788E-004,0.0)
p=5	(2.857224908432099E-004,0.0)

Table 3. Gabor expansion coefficients for a narrow half-wavelength high aperture illuminated by sinusoidal field distribution ($L_{ox}/L_x = \lambda/2 = L_{oy}/L_y = \lambda/200$) and $n=q=0$, $|m|,|p| \leq 5$

CHAPTER 6

CONCLUSIONS

The Gabor representation in the context of a two dimensional aperture problem has been summarized in this work. It is an expansion for a radiated field in terms of a discrete set of linearly shifted and spatially rotated elementary Gaussian beams. The parameters that can be varied in this summation are the number of beams and corresponding beam widths. The validity of the narrow beam algorithm with almost a priori predictability has been reconfirmed for one and two dimensional apertures. The equivalent dipole antenna concept based on narrow aperture has been described and its validity through application of Gabor representation has been confirmed. Here, the Gabor representation has been applied to a narrow rectangular aperture illuminated with a sinusoidal field. The narrow aperture ($height >> width$) excited by sinusoidal field distribution approximates an equivalent dipole with a similar current distribution with only exception that aperture radiates into a half-space whereas the dipole covers the entire space. Utilizing the narrow beam algorithm, once the expansion coefficients were determined, the radiated electric field potential in near, mid and far zones were evaluated. The criteria in determining the number of expansion coefficients based on re-generation of the aperture field distribution with sufficient accuracy has been demonstrated. It was observed that even though wide beam algorithm was applied, less number of terms resulted in erroneous side lobes and higher number of terms caused Gibbs phenomena in the region close to the aperture plane.

The numerical evaluations are carried out for the half-wavelength high narrow aperture. Far zone numerical results of radiated potential utilizing Gabor expansion are compared to analytical expressions determined via Fourier transform. The unique application developed in this work in expressing the radiated field of an equivalent dipole antenna revealed that Gabor expansion can be a valuable tool in studying radiation from practical sources such as open ended waveguides, horns and other aperture type radiators.

REFERENCES

1. Gabor, D. "Theory of Communications." *J. Inst. Elec. Eng.* 93III (1946): 429-457.

2. Bastiaans, M. J. "The Expansion of an Optical Signal into a Discrete Set of Gaussian Beams." *Optik* 57 (1980) No.1.

3. Bastiaans, M. J. "A Sampling Theorem for the Complex Spectrogram and Gabor's Expansion of A Signal in Gaussian Elementary Signals." *Optical Engineering* 20 (1981): 594.

4. Janssen, A. J. E. M. "Gabor Representation of Generalized Functions." *J. Math. Anal. Appl.* 83 (1984): 377-394.

5. Einzinger, P. D. , Raz, S., and Shapira, M. " Gabor Representation and Aperture Theory." *J. Opt. Soc. Am.* A/Vol 3. No.4,(1986): pp508-522.

6. Maciel, J. J., and Felsen, L. B. "Systematic Study of Fields Due to extended Apertures by Gaussian Beam Discretization." *IEEE Transactions on Antennas and Propagation* AP-37 (1989):884-892.

7. Niver, E., and Birand, T. "Application of Spherical Wave Theory to Rectangular Apertures." *AEU Electronics and Communications* Band 29 (1975):96-99.

8. Jackson, J.D. 1962. *Classical Electrodynamics* New York: J.Wiley and Sons.